NASA/TM—2003-212347

Simulation of the Flow Field Associated With a Rocket Thruster Having an Attached Panel

Farhad Davoudzadeh
University of Toledo, Toledo, Ohio

Nan-Suey Liu
Glenn Research Center, Cleveland, Ohio

May 2003

The NASA STI Program Office . . . in Profile

Since its founding, NASA has been dedicated to the advancement of aeronautics and space science. The NASA Scientific and Technical Information (STI) Program Office plays a key part in helping NASA maintain this important role.

The NASA STI Program Office is operated by Langley Research Center, the Lead Center for NASA's scientific and technical information. The NASA STI Program Office provides access to the NASA STI Database, the largest collection of aeronautical and space science STI in the world. The Program Office is also NASA's institutional mechanism for disseminating the results of its research and development activities. These results are published by NASA in the NASA STI Report Series, which includes the following report types:

- TECHNICAL PUBLICATION. Reports of completed research or a major significant phase of research that present the results of NASA programs and include extensive data or theoretical analysis. Includes compilations of significant scientific and technical data and information deemed to be of continuing reference value. NASA's counterpart of peer-reviewed formal professional papers but has less stringent limitations on manuscript length and extent of graphic presentations.

- TECHNICAL MEMORANDUM. Scientific and technical findings that are preliminary or of specialized interest, e.g., quick release reports, working papers, and bibliographies that contain minimal annotation. Does not contain extensive analysis.

- CONTRACTOR REPORT. Scientific and technical findings by NASA-sponsored contractors and grantees.

- CONFERENCE PUBLICATION. Collected papers from scientific and technical conferences, symposia, seminars, or other meetings sponsored or cosponsored by NASA.

- SPECIAL PUBLICATION. Scientific, technical, or historical information from NASA programs, projects, and missions, often concerned with subjects having substantial public interest.

- TECHNICAL TRANSLATION. English-language translations of foreign scientific and technical material pertinent to NASA's mission.

Specialized services that complement the STI Program Office's diverse offerings include creating custom thesauri, building customized databases, organizing and publishing research results . . . even providing videos.

For more information about the NASA STI Program Office, see the following:

- Access the NASA STI Program Home Page at ***http://www.sti.nasa.gov***

- E-mail your question via the Internet to help@sti.nasa.gov

- Fax your question to the NASA Access Help Desk at 301–621–0134

- Telephone the NASA Access Help Desk at 301–621–0390

- Write to:
  NASA Access Help Desk
  NASA Center for AeroSpace Information
  7121 Standard Drive
  Hanover, MD 21076

NASA/TM—2003-212347

Simulation of the Flow Field Associated With a Rocket Thruster Having an Attached Panel

Farhad Davoudzadeh
University of Toledo, Toledo, Ohio

Nan-Suey Liu
Glenn Research Center, Cleveland, Ohio

Prepared for the
2003 Fluids Engineering Division Summer Meeting
cosponsored by the American Society of Mechanical Engineers
and the Japan Society of Mechanical Engineers
Honolulu, Hawaii, July 6–10, 2003

National Aeronautics and
Space Administration

Glenn Research Center

May 2003

Acknowledgments

The authors appreciate Mr. Kevin Dickens for providing the experimental data and
Dr. Ananda Himansu for his very helpful comments and discussions during the course of this work.

Available from

NASA Center for Aerospace Information
7121 Standard Drive
Hanover, MD 21076

National Technical Information Service
5285 Port Royal Road
Springfield, VA 22100

Available electronically at http://gltrs.grc.nasa.gov

SIMULATION OF THE FLOW FIELD ASSOCIATED WITH A ROCKET THRUSTER HAVING AN ATTACHED PANEL

Farhad Davoudzadeh
University of Toledo
Toledo, Ohio 43606

Nan-Suey Liu
National Aeronautics and Space Administration
Glenn Research Center
Cleveland, Ohio 44135

Abstract
The NCC [1] code has been used to predict the supersonic flows associated with the hot gas exhaust of a H2-O2 thruster under a variety of hot fire conditions. The 2-D computational domain includes part of the combustion chamber, the converging- diverging square nozzle, and a flat panel attached to the lower surface of the nozzle exit. The predicted flow features include a system of shocks, extended hot plumes, the computed surface pressure, and the surface temperature along the 'adiabatic' flat panel. The measured surface pressure and surface temperature along the 'cooled' panel are also presented.

1. Experimental Setup and the Geometry

The experimental set-up together with the rocket thruster is shown in Figure 1. A perspective view of the geometry is shown in Figure 2. The geometry is symmetrical about a vertical plane along the flow direction, as shown in Figure 2. It begins from midsection of the combustor, 0.22m ahead of the nozzle's throat. The combustion chamber is a square duct. It is connected to a converging-diverging nozzle with an exit area ratio (Ae/At) of 1.85. A diving board and a flat panel (calorimeter) extend from the lower surface of the diverging nozzle [2]. Two vertical walls forming an open channel bound the diving board and the flat panel. Pipes circulating cold water, cool the thruster, the sidewalls, and the flat panel, as shown in Figure 1.

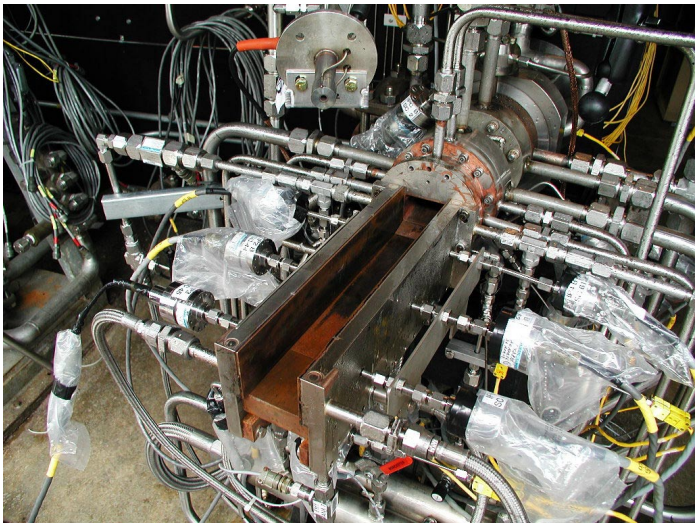

Figure 1. The thruster assembly

2. Computational Domain

The computational domain is two-dimensional, with the boundaries being located very far from the body of the thruster to minimize the influences of the imposed boundary conditions on the thruster flow. In particular, the exit boundary is approximately fifteen meters downstream of the nozzle's exit, whereas the body length is approximately 0.62m. This is to ensure that the computational domain contains the whole extent of the supersonic flow and that the flow is subsonic at the exit plane. A close-up of the computational domain, together with the grid distribution is shown in Figure 3.

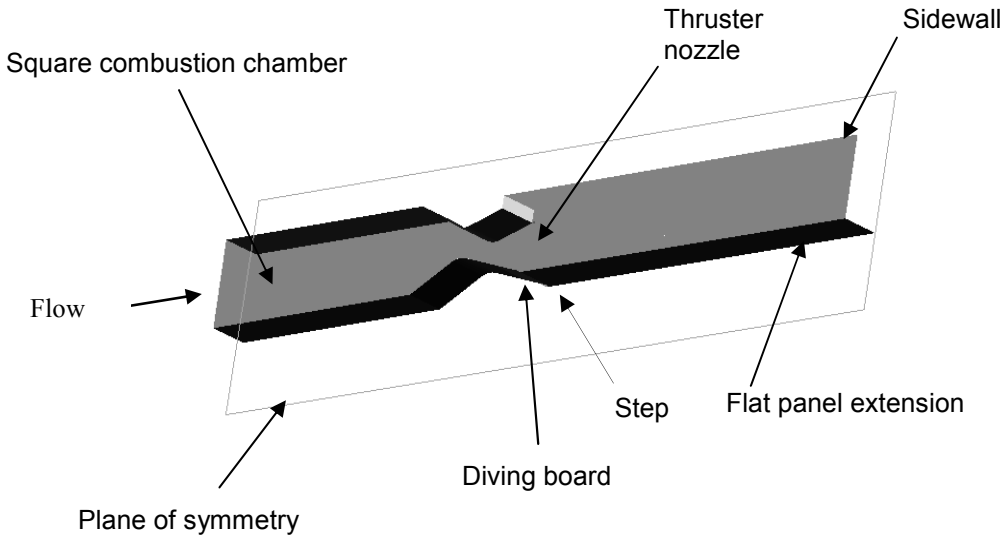

Figure 2. Geometry of the thruster about the plane of symmetry

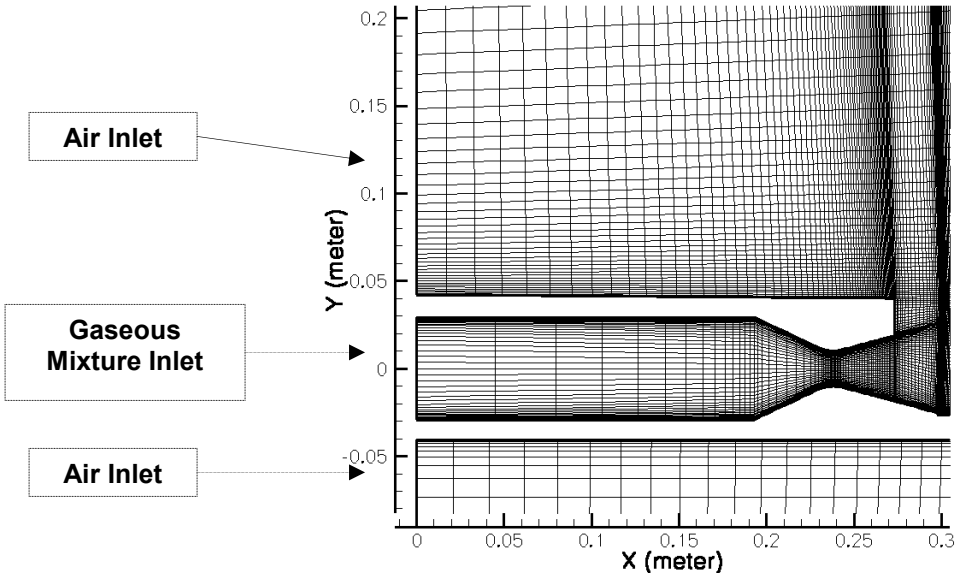

Figure 3. Close-up of the computational domain and the grid distribution

3. Boundary Conditions

The specified inlet boundary condition for the combustion chamber is: fixed inlet velocity, density and temperature. The input for the chemistry model, mole fractions and the properties of the combustion products are obtained from the NASA Glenn's Chemical Equilibrium program (CEA). It should be noted that the combustion is not simulated in the present effort. The simulation is initiated with the combustion already complete. The fuel is gaseous H2 and the oxidizer is gaseous O2. The product of the combustion is a mixture of gaseous H, HO2, H2, H2O, H2O2, O, OH, and O2. The mole fractions of these constituents are obtained from the CEA code and are used to setup the mass fraction of the mixture.

The exit boundary is specified to be subsonic, and at ambient pressure.

The top and the bottom boundaries are far enough from the thruster that their influences on the nozzle flow are negligible, for this reason and for minimizing grid points, these boundaries are specified as symmetry planes which are similar to inviscid walls.

The left side boundaries above and below the combustion chamber's inlet are air inlets (see figure 3) with specified velocity, density, and temperature. The incoming fluid on these boundaries are assumed to be air, with the velocity of approximately 6% that of the inlet velocity of the mixture into the combustion chamber. This is done to account for the entrainment induced by the plume for which no experimental value is measured. Along the walls, an adiabatic condition is applied. For viscous flows, non-slip wall condition is used, while slip wall condition is used in inviscid flows.

4. Grid Refinement

Several Navier-Stokes calculations are performed to determine the effects of the proximity of the boundaries and the grid resolution on the flow field. To account for the grid resolution effects, the grid is refined several times until no noticeable change in the computed flow field occurred; and the final refined grid is used for the detailed computations. Figure 4 shows the computed Mach number distribution for a refined grid of the Case Pc500—this case will be discussed in detail later. Superimposed on Figure 4 are variation of the absolute pressure in the centerline passed the nozzle exit and along the flat panel for a coarse grid (24,439 element) and a fine grid (65,183 element). Clearly the fine grid captures more details of the flow variable quantities-here the absolute pressure-in the high flow gradient regions across the shocks. In other areas, the coarse grid and the fine grid results are identical. The results presented here are for the final refined grid.

5. Description of the Simulation Cases

Using the National Combustion Code (NCC), four different cases are numerically simulated. The inlet boundary conditions for these cases are presented in Tables 1 and 2. The gaseous species and their mole fractions shown in Table 2 are obtained from the CEA code.

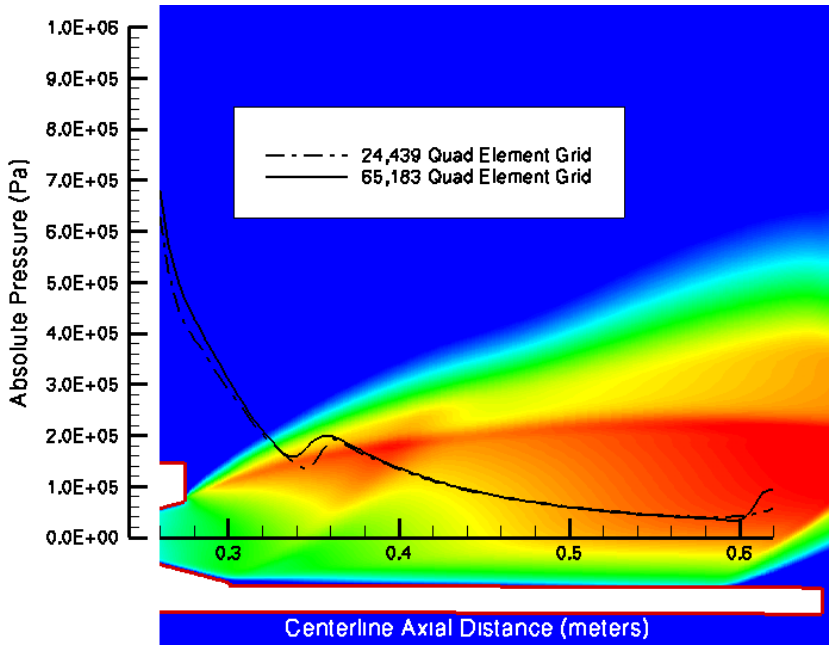

Figure 4. Grid refinement effects

Table 1. Inlet condition for different simulations

Simulation Case	Combustion Chamber Pressure (psia)	Combustion Chamber Temperature (°K)	Density (Kg/m^3)	Gaseous mixture
Case Pc500	500	3564.64	1.687	H, HO2, H2, H2O, H2O2, O, OH, O2
Case Pc300	300	3202.67	0.83408	H,H2,H2O,O,OH,O2
Case Pc250	250	3184.96	0.69801	H,H2,H2O,O,OH, O2
Case Pc130	130	2065.47	0.31552	H,H2,H2O,OH

Table 2. Inlet gaseous mixture and mole fractions for different simulations

Case Pc500		**Case Pc300**		**Case Pc250**		**Case Pc130**	
Gaseous species	**Mole fractions**	**Gaseous mixture**	**Mole fractions**	**Gaseous mixture**	**Mole fractions**	**Gaseous mixture**	**Mole fractions**
H	0.04898	**H**	0.03998	**H**	0.04169	**H**	0.00073
HO2	0.00011	**H2**	0.41148	**H2**	0.41054	**H2**	0.74738
H2	0.17736	**H2O**	0.5272	**H2O**	0.52370	**H2O**	0.25187
H2O	0.65444	**O**	0.00114	**O**	0.00123	**OH**	0.00003
H2O2	0.00002	**OH**	0.01963	**OH**	0.02022		
O	0.01373	**O2**	0.00057	**O2**	0.00062		
OH	0.08595						
O2	0.01942						
Oxidizer Fuel Ratio (o/f) = 7.0		**o/f = 4.5**		**o/f = 4.5**		**o/f = 2.0**	

6. Case Pc500 Results

Case Pc500 has the most diverse flowfield characteristics, so this case is described in detail first. Analyses of the other three cases are summarized later. All cases are computed using a 65,183-element grid.

6.1. Viscous Results

To demonstrate the effects of viscous layer on the computed quantities on the flat panel, viscous and inviscid calculations are performed. Viscous simulation results are presented first, followed by inviscid results.

6.1.1. The Plume

Figure 5 shows the Mach number distribution for the entire domain, for the steady state solution. A plume created by the flow leaves the combustor at approximately 16 degrees. It extends over the entire length of the domain. A significant portion of the plume is supersonic.

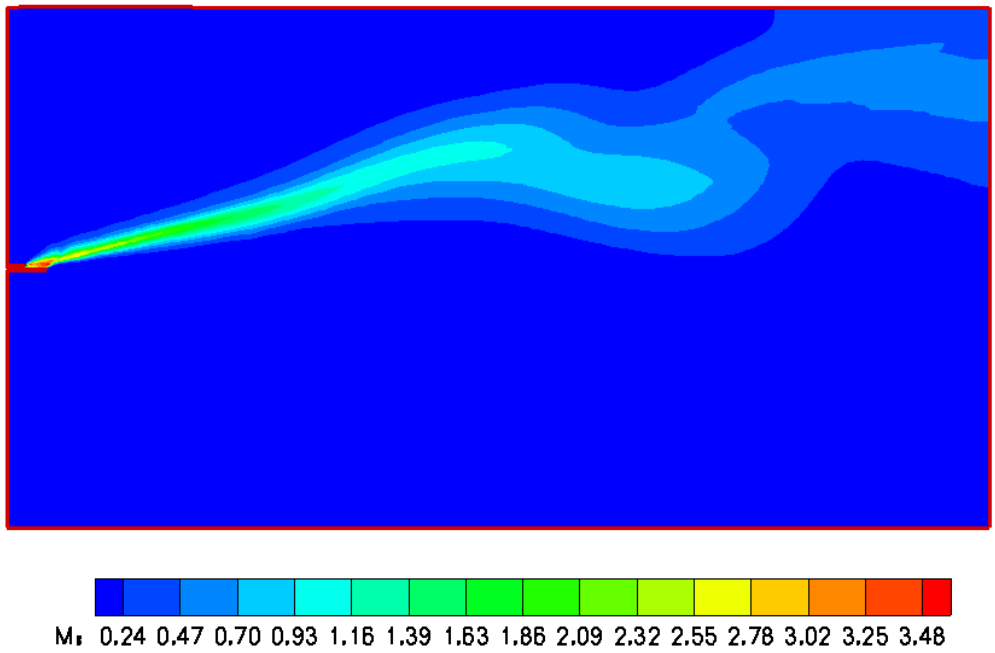

Figure 5. Mach number distribution

A close-up of the Mach number distribution, in the vicinity of the nozzle's exit is shown in Figure 6. The temperature field for the computational domain is shown in Figure 7. The temperature remains high along the plume for a long distance.

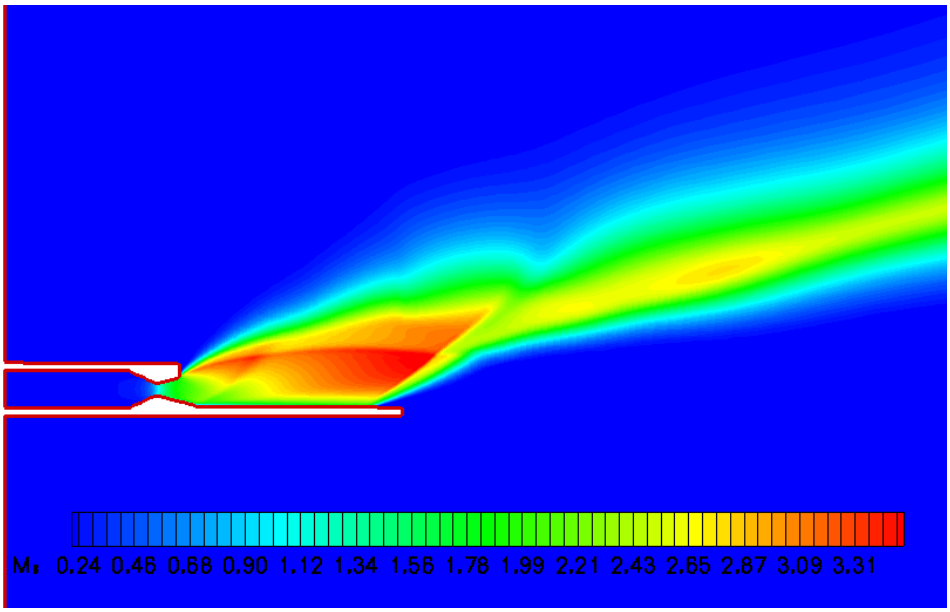

Figure 6. Close-up of the Mach number distribution

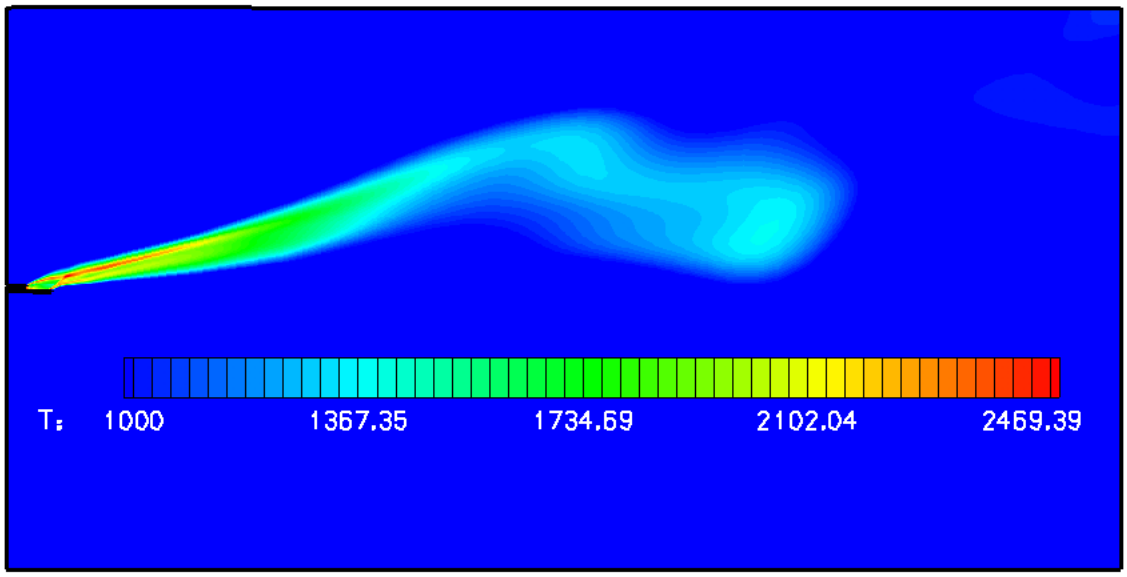

Figure 7. Computed temperature (°K) distribution

A close-up of the temperature field is shown in Figure 8.

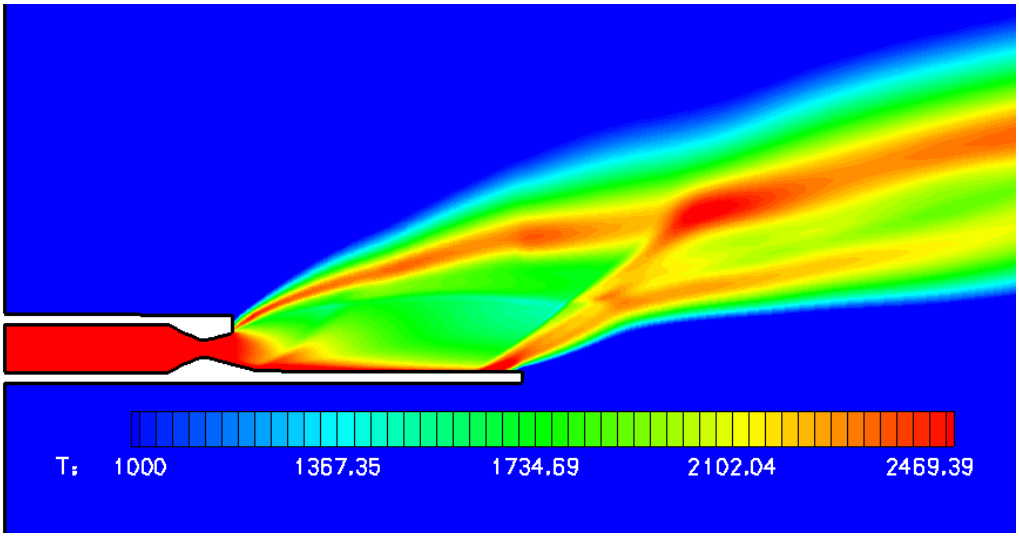

Figure 8. Close-up of temperature (°K) distribution

6.1.2. Oblique Shock Waves

Examination of the flow field reveals formation of at least three oblique shock waves, as shown in Figure 9. The first shock line is formed at the end of the inclined ramp where the supersonic flow, coming off the nozzle, is forced to change direction. Note the formation of a re-circulation zone in the step that separates the diving board and the flat panel. The second shock line, which is much stronger, is formed towards the end of the horizontal flat panel where a relatively large back pressure is imposed on the supersonic flow by the downstream ambient conditions. In front of this shock the boundary layer increases in thickness. The adverse pressure gradient created by the shock is sufficient to cause the flow separation, as evidenced in the inset. This shock makes an angle of approximately 36 degrees with the panel, and directs the flow upward. The flow between the first shock and the second shock is still highly supersonic and is being forced upwards by the second shock. As it faces the relatively large ambient back pressure outside the jet and above the flat panel, it adjusts to the ambient pressure via the creation of the third shock, which starts from the upper edge of the nozzle's exit and extends downstream, above and along the bottom flat panel. This third shock directs the flow towards the right. The flow directed by the second and the third shock is forced to leave the shock system above the panel at approximately 16 degrees as it enters the ambient air.

The insets on the Figure 9 show the velocity vectors, superimposed on the Mach number distributions, at the locations indicated by the arrows.

Figures 10 through 12 show the Mach number distribution, the pressure distribution and the density distribution from the combustion chamber through out the flat panel. Superimposed on these figures are the line plots of these variables as a function of the distance along the centerline of the nozzle. The discontinuities of the fluid properties on the shock lines can be discerned from these figures. It should be noted that effective viscosity, heat conduction, mass diffusion, grid density and numerical dissipation effects tend to smooth out the discontinuities.

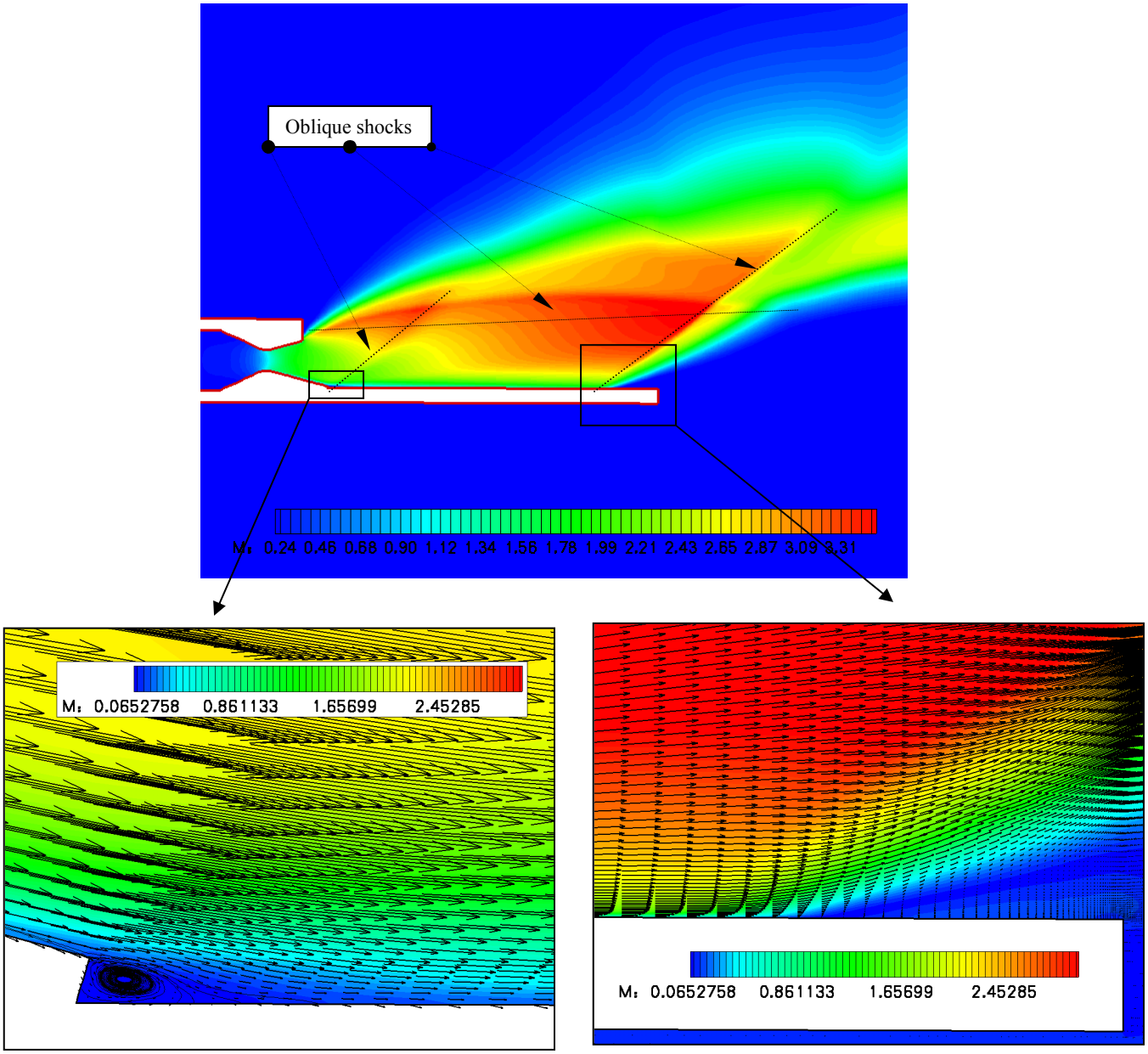

Figure 9. Mach number distribution, shock waves, and boundary layer separation

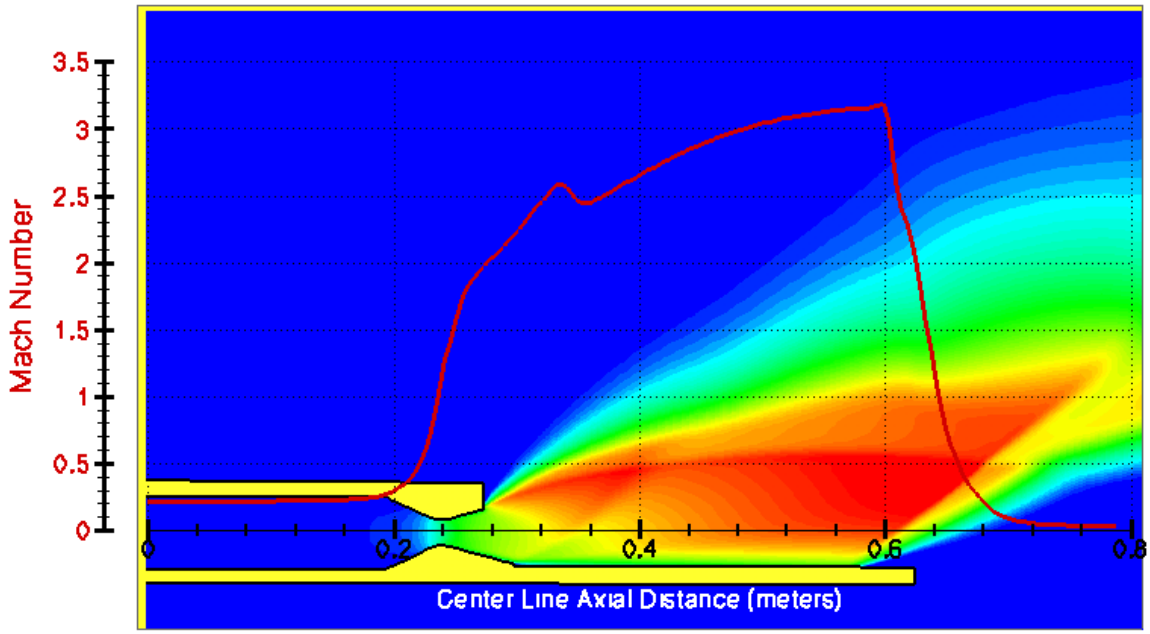

Figure 10. Mach number distribution, and Mach number variation as a function of position along the centerline

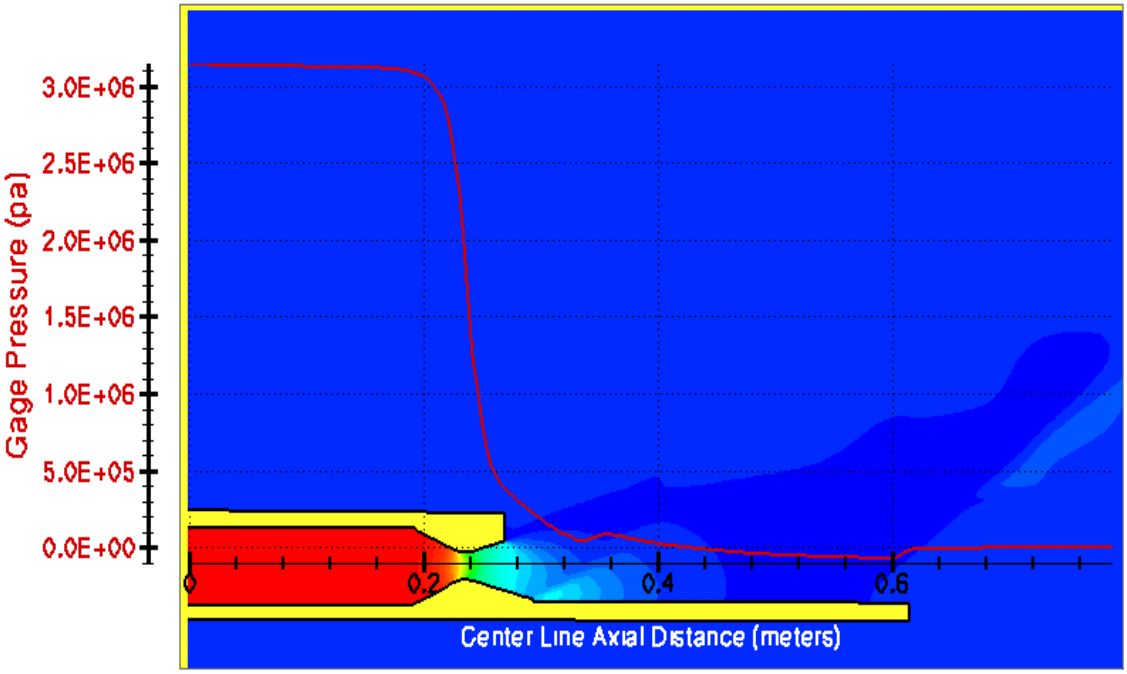

Figure 11. Pressure (gage) distribution, and pressure variation as a function of position along the centerline

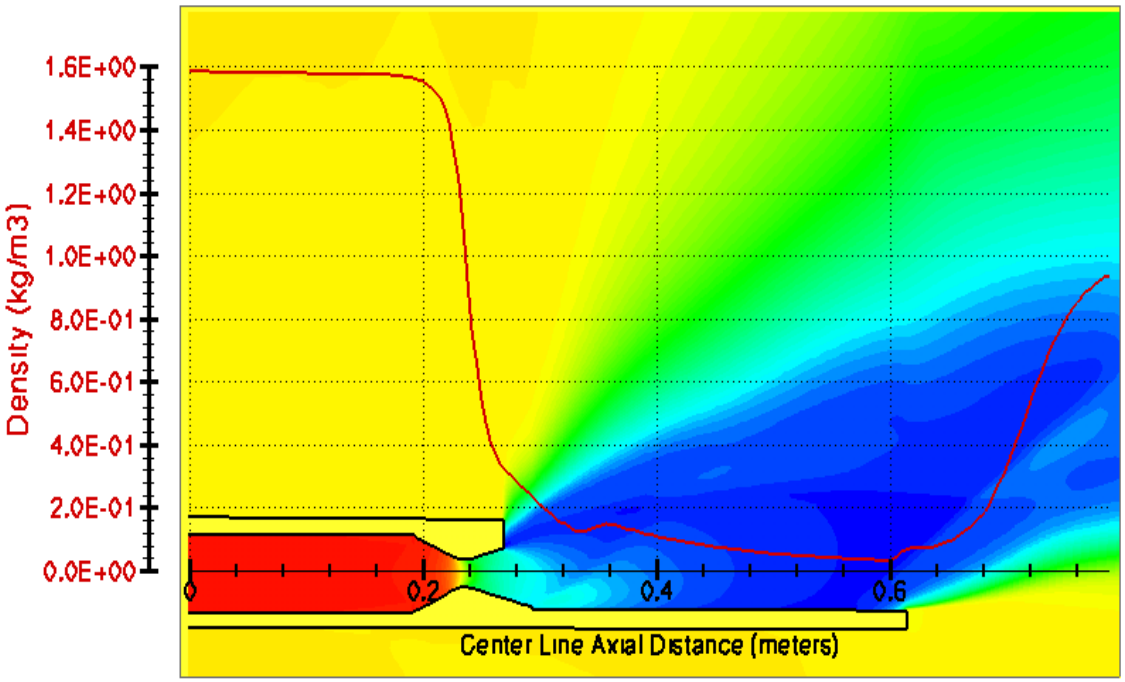

Figure 12. Density distribution, and density variation as a function of position along the centerline

6.2 Inviscid Results

To determine the effects of the viscous boundary layer on the formation and the location of the shocks, and on the wall temperature and pressure, a computation is performed solving the Euler equations, where the viscous terms are not considered.

Distribution of the Mach number for inviscid results is shown in Figure 13. Note that the second shock is moved farther down to the end of the flat panel.

Furthermore, since there are no viscous effects, the shocks are not diffused and therefore, are better defined. Figures 13 and 14 show the sudden change in the value of the Mach number and density along the lower wall, as the flow passes through the shock waves. Also, note the sharp variation of the inviscid flow behavior near the diving board.

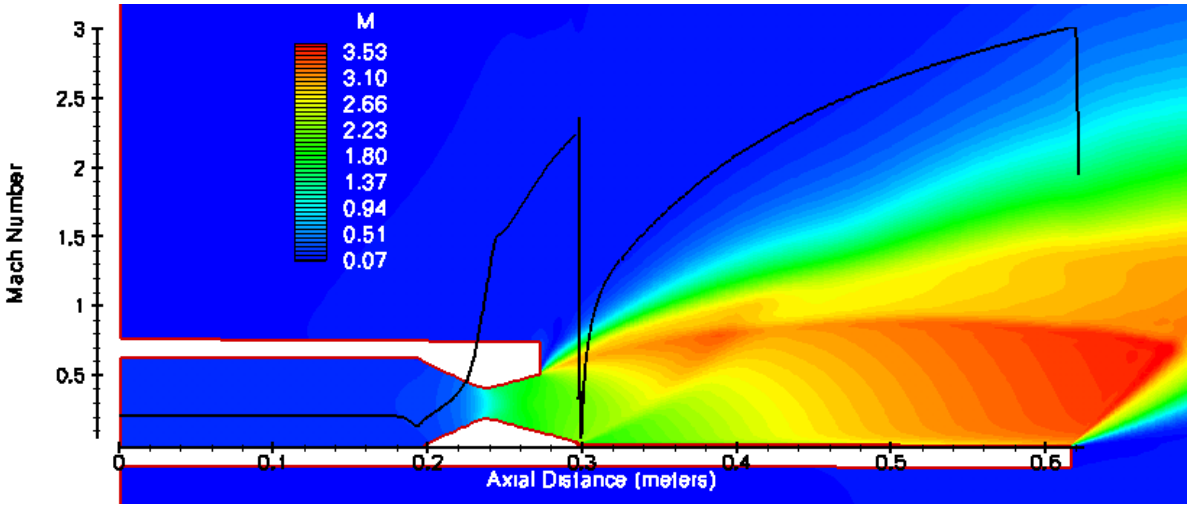

Figure 13. Mach number distribution, and Mach number variation along the lower wall for the inviscid simulation

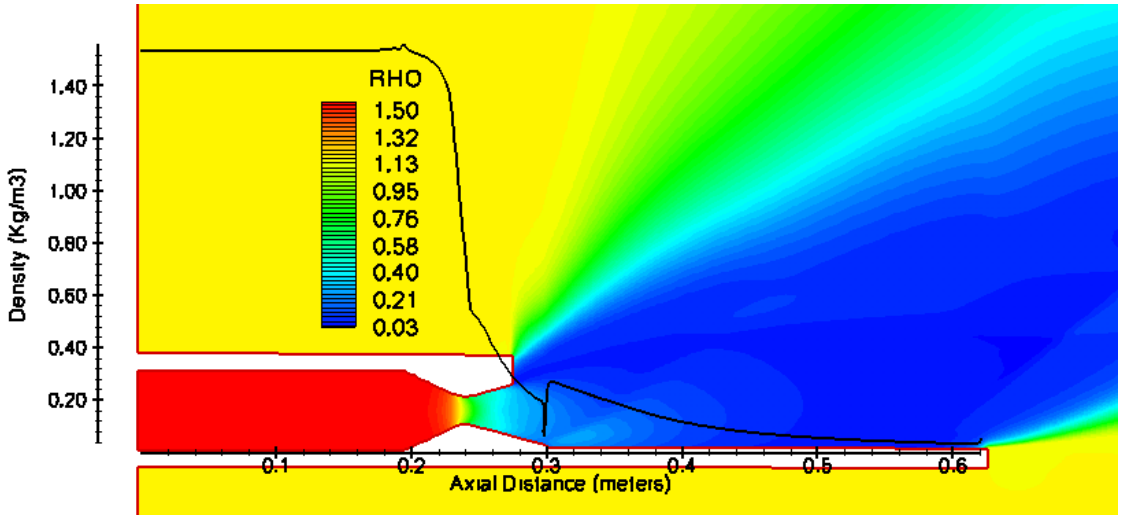

Figure 14. Density distribution, and density variation along the lower wall for the inviscid simulation

6.3 Wall Temperature and Pressure

One of the goals of this study has been to determine the pressure and temperature distribution on the lower wall surface, particularly that of the inclined ramp and the flat panel attached to it. For the adiabatic wall condition, the temperature distributions along the lower surface, starting from the inlet section, and ending on the end of the flat panel, for the viscous and for the inviscid results are shown in Figures 15 and 16, respectively. The presence of the boundary layer in the viscous calculations results in much higher wall temperature than the inviscid calculation. Contours of temperature close to the walls of the inclined ramp and the flat panel are shown if Figure 17. The contour levels for this figure are clipped between 2200 and 2976K, to exhibit the temperature distribution and variation close to these walls.

Note the jump in the magnitude of the temperature immediately aft of the shock, near the end of the flat panel. In the case of the viscous results (Figure 15), this jump in temperature is followed by a steep drop, due to the boundary layer separation towards the end of the flat panel. In the inviscid case (Figure 16), no separation has taken place on the panel and the temperature stays high.

The pressure distribution on the walls for both viscous and inviscid results is practically identical. The pressure (gage) distribution is shown in Figure 18. A more detailed close-up of the pressure distribution illuminating the effects of the shock lines is given in Figure 19.

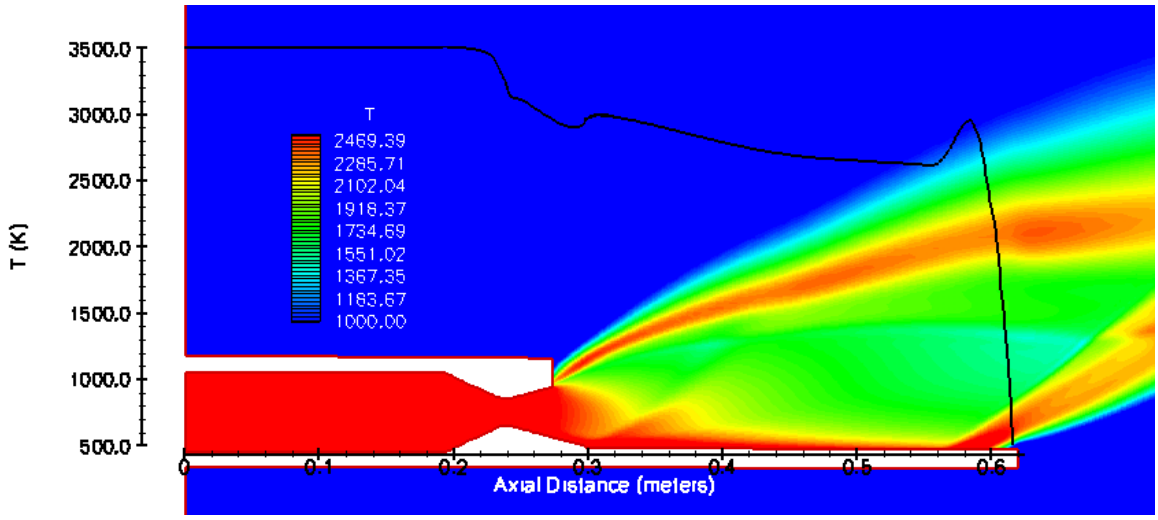

Figure 15. Temperature distribution, and temperature variation along the lower wall, viscous result

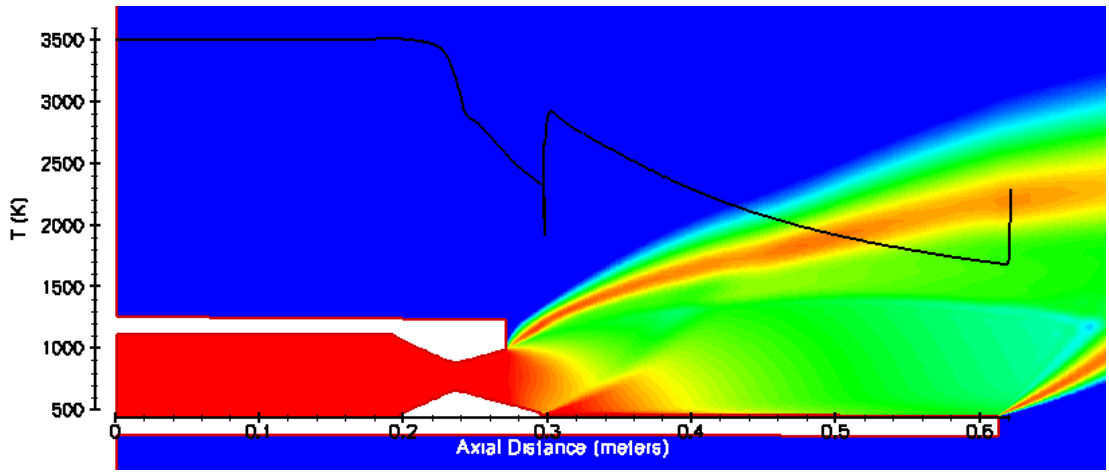

Figure 16. Temperature distribution, and temperature variation along the lower wall, inviscid result

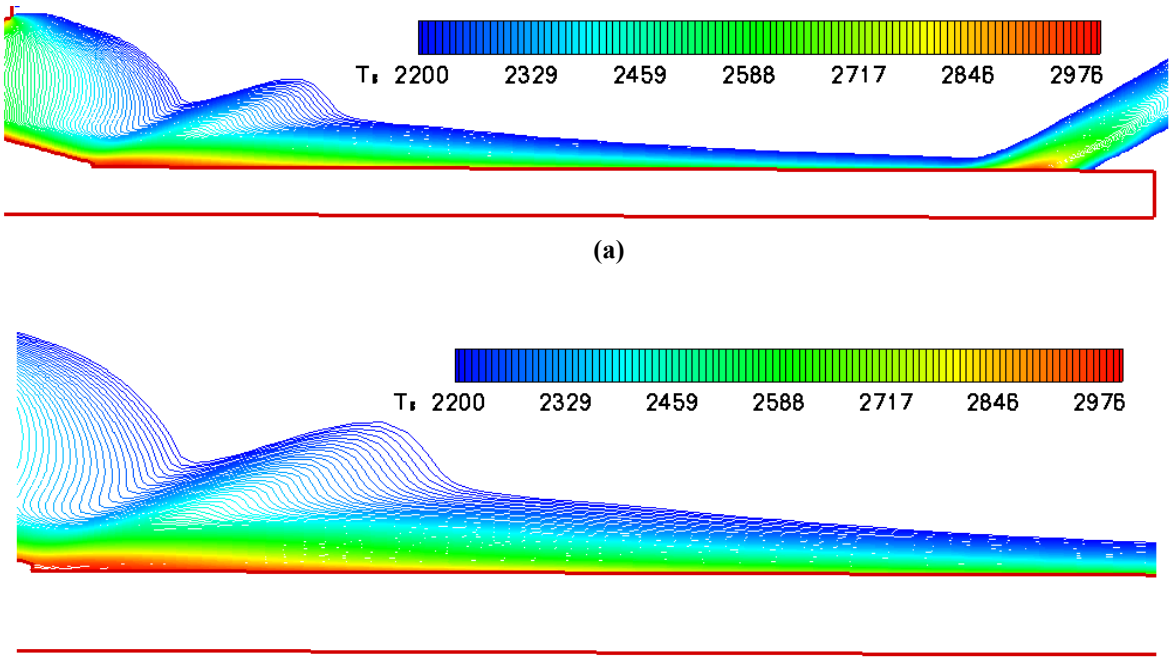

Figure 17. Contours of temperature distribution along the inclined ramp and the flat panel, viscous result

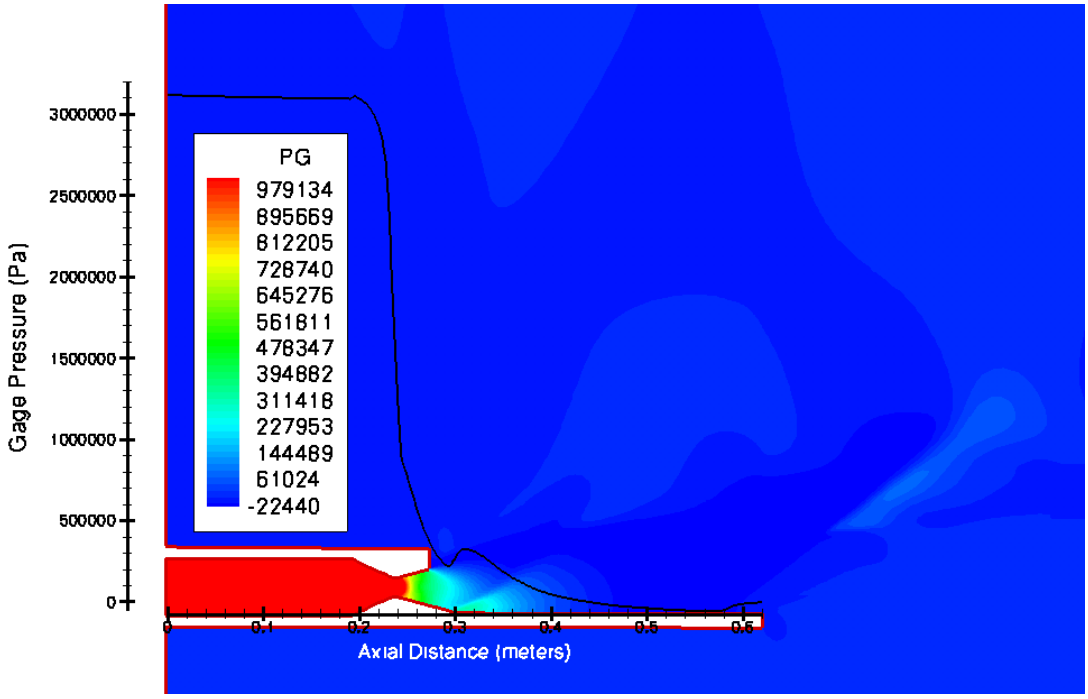

Figure 18. Pressure distribution, and pressure variation along the lower wall

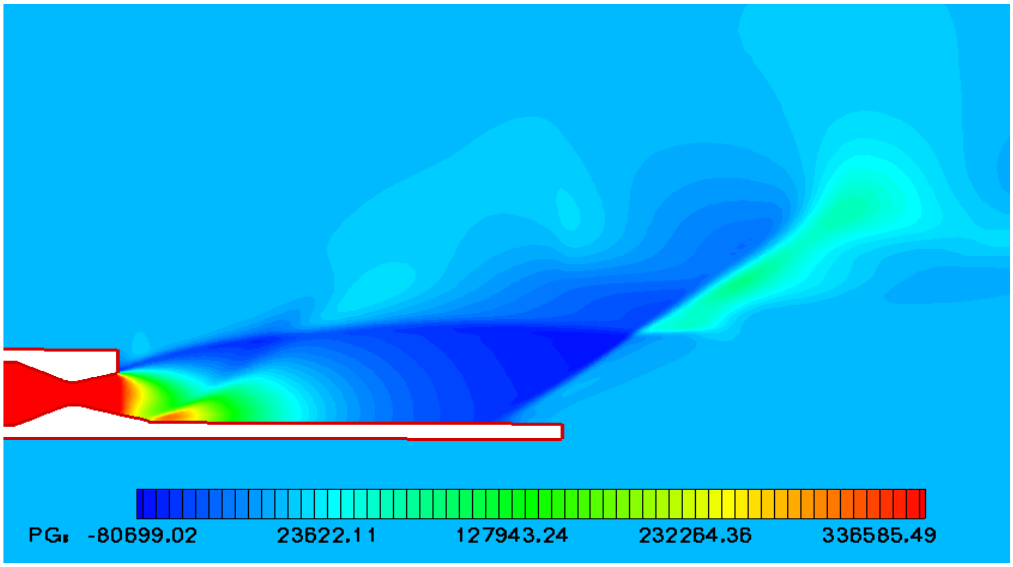

Figure 19. Pressure distribution for the viscous simulation

7. Cases Pc300, Pc250, and Pc150 Results

Figure 20 shows the Mach number distribution for the four cases. The operating conditions for these cases are given in Tables 1 and 2. The extent and the direction of the plumes for different operating conditions are also shown in this figure. The Case Pc500 exhibits the highest plume angle. This is the case where the Mach number remains very high past the initial shock, aft of the inclined ramp, and over the flat panel. The close-ups of the Mach number distributions, demonstrating the structure of the shocks, are shown in Figure 21. Distribution of the computed pressure on the surface of the flat panel and its related measurement are also shown in this figure.

Absolute pressure distribution and temperature distribution for all the cases are given in Figures 22 and 23. These figures also show the distribution of pressure and temperature on the flat panel.

Beyond the nozzle exit, the geometry is asymmetric about the nozzle centerline; and as a result, the shock patterns are not symmetric. The amount of asymmetry in the shock pattern is a function of the velocity of the jet exiting the nozzle. In the case of the Pc130, the exit velocity is not high enough to create excessive asymmetry about the centerline of the nozzle. The typical diamond shaped shock pattern still can be recognized. Two shocks originating from the corners of the exit, cross one another, with the one originating from the top corner and directed towards the bottom surface, deflecting on the flat panel and creating a weaker shock. The rise in the wall pressure shown in the curve of Figure 21(d) demonstrates the effect of the deflected shock. As the chamber pressure and consequently the exit velocity increases, the asymmetry becomes more pronounced to the degree that the shock emanating from the top edge of the nozzle exit is directed away from the panel as is in the case of the Pc300 shown in Figure 21(b) and eventually it is parallel to the flat panel as is in the case of the Pc500 shown in Figure 21(a). However, since this shock is directed away from the panel, the flow underneath it is still highly supersonic and as it approaches the end of the panel, it encounters the large ambient pressure and reacts to it by creating the third shock anchored to the surface. This third shock, in the case of the Pc500 is strong enough to defect the flow to create the plume that leaves the panel at approximately 16 degree.

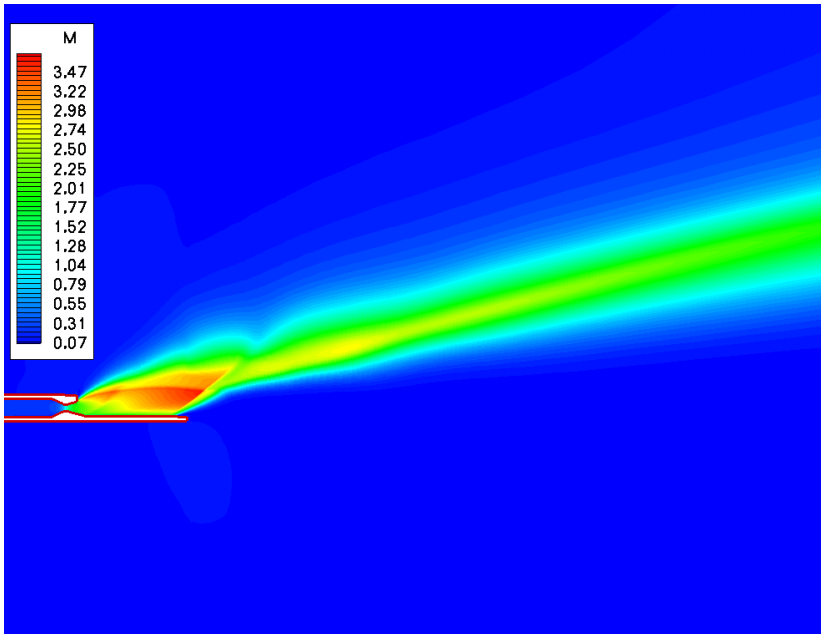

(a) Pc500

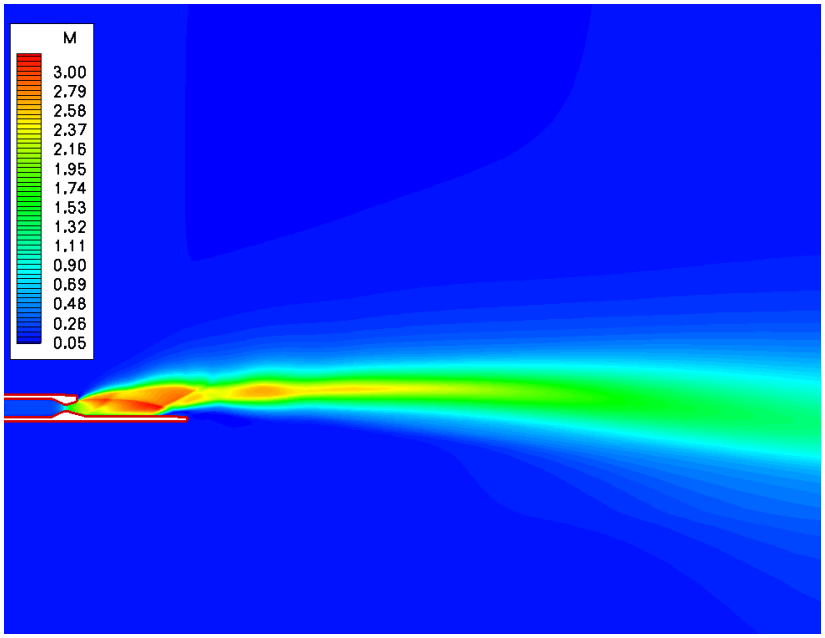

(b) Pc300

Figure 20 (a-b). Mach number distribution and the plume direction for the Pc500, Pc300 cases

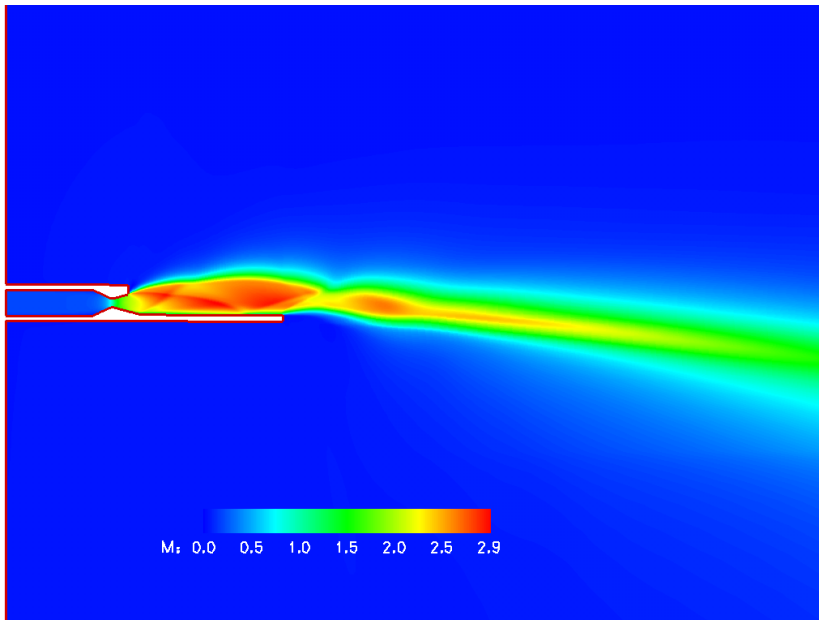

(c) Pc250

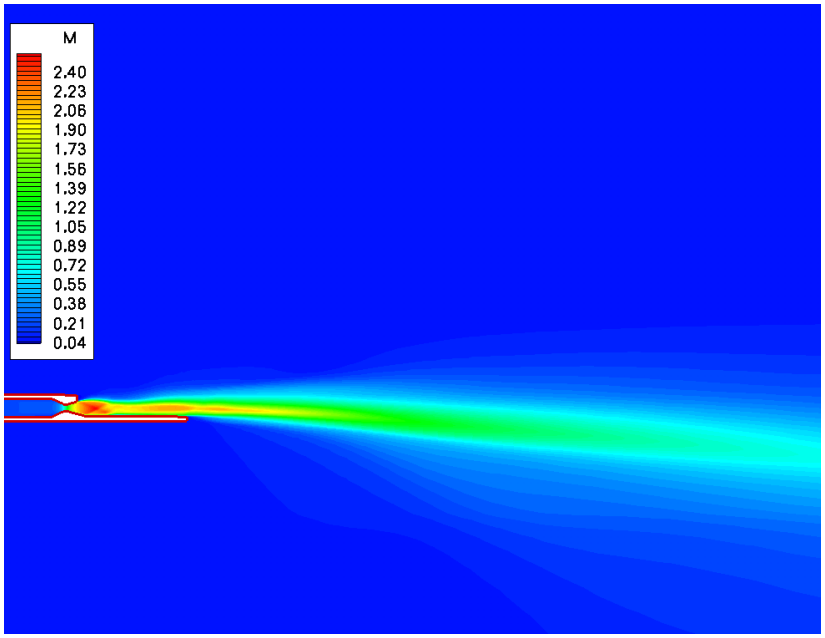

(d) Pc130

Figure 20 (c-d). Mach number distribution and the plume direction for the Pc250, Pc130 cases

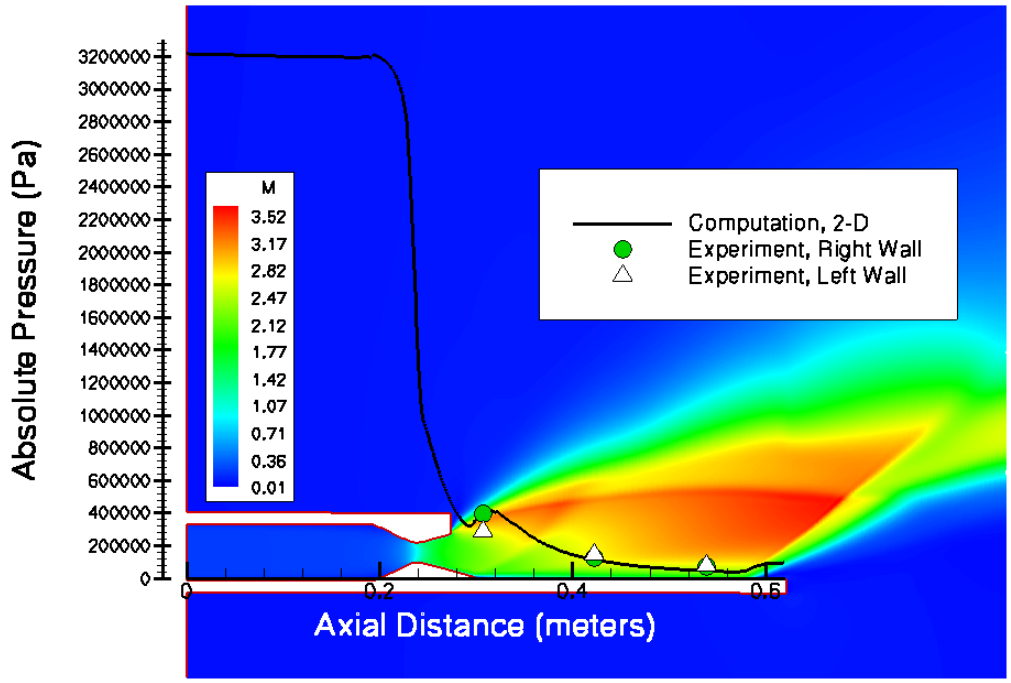

(a) Pc500 – Combustion Chamber Pressure = 500 psia

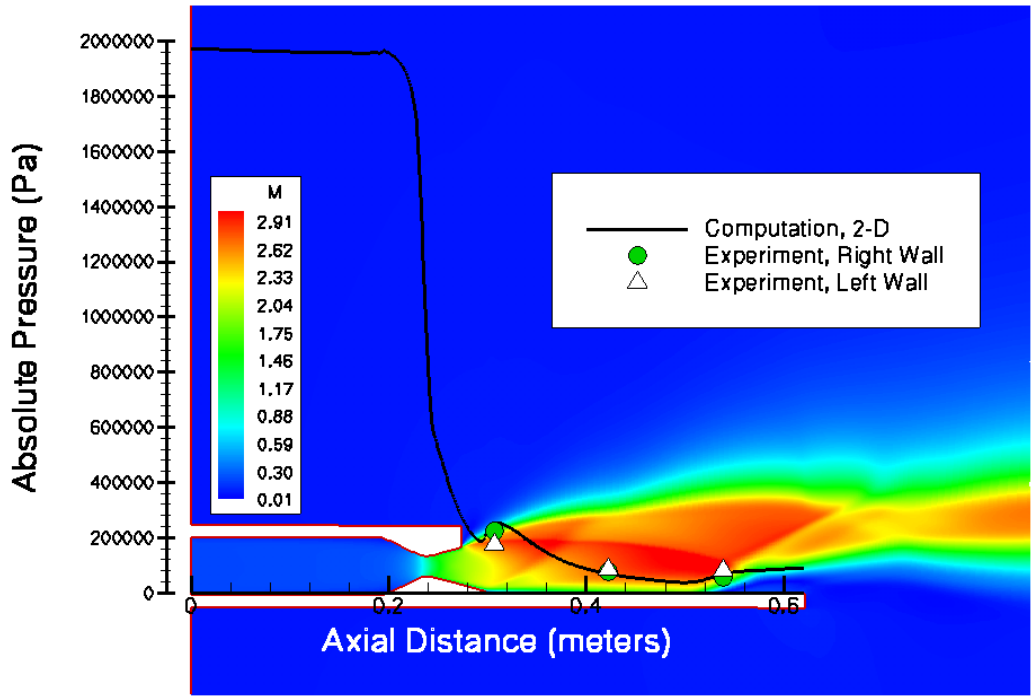

(b) Pc300 – Combustion Chamber Pressure = 300 psia

Figure 21 (a-b). Mach number contours, computational pressure distribution, and related experimental measurement along the wall for Pc500 and Pc300 cases

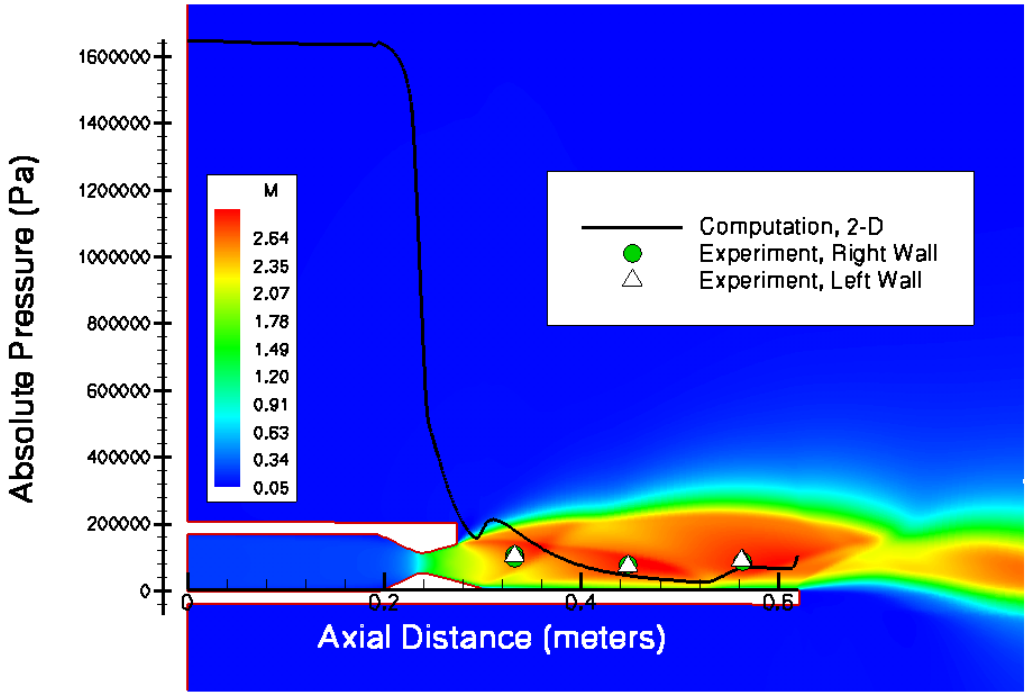

(c) Pc250 – Combustion Chamber Pressure = 250 psia

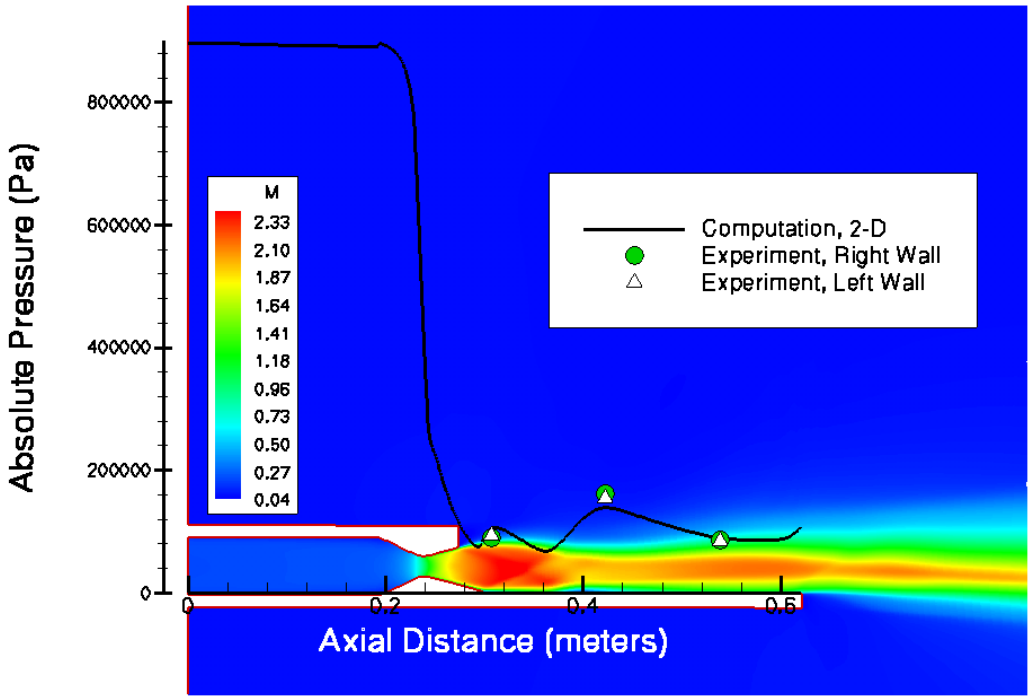

(d) Pc130 – Combustion Chamber Pressure = 130 psia

Figure 21 (c-d). Mach number contours, computational pressure distribution, and related experimental measurement along the wall for the Pc250 and Pc130 cases

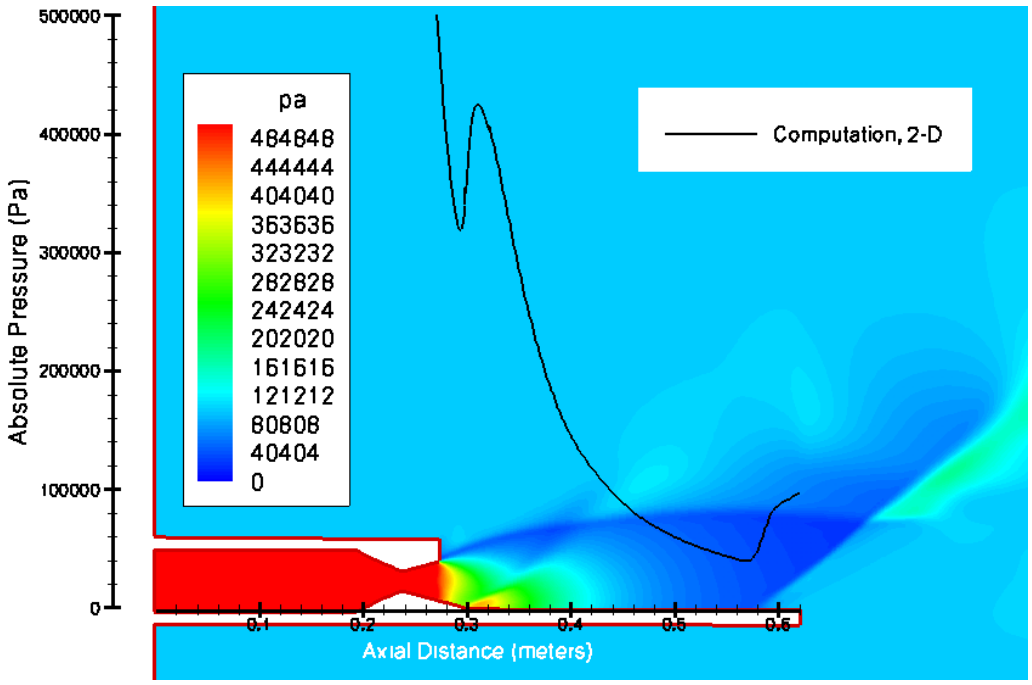

(a) Pc500 – Combustion Chamber Pressure = 500 psia

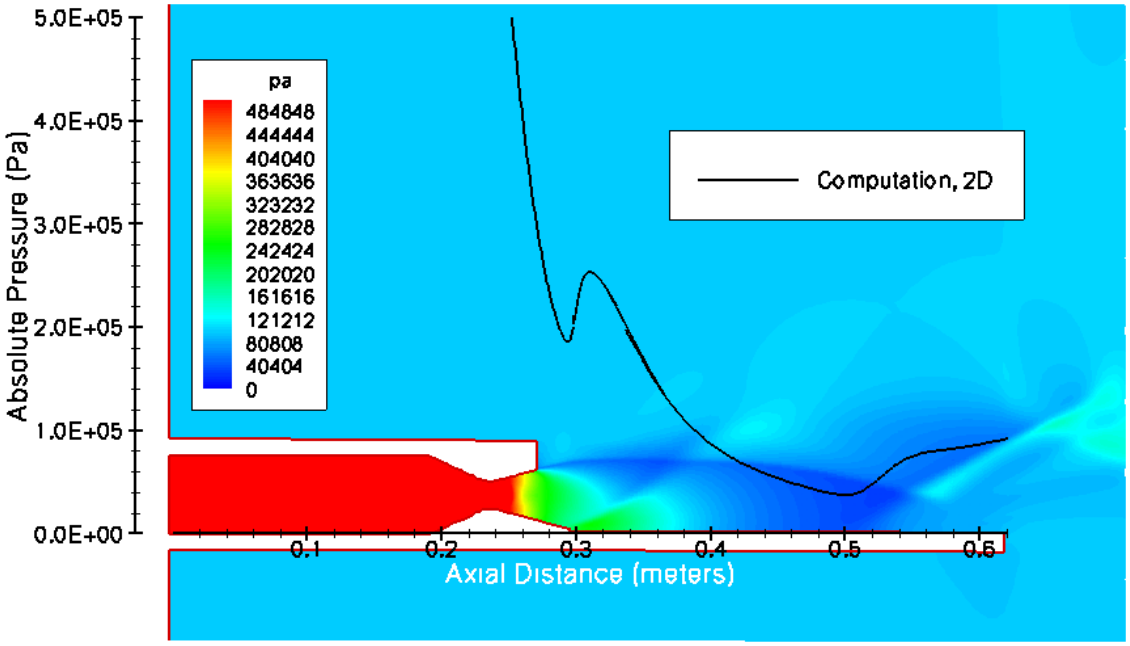

(b) Pc300 – Combustion Chamber Pressure = 300 psia

Figure 22 (a-b). Pressure contours and pressure distribution along the wall for Pc300 and Pc500 cases

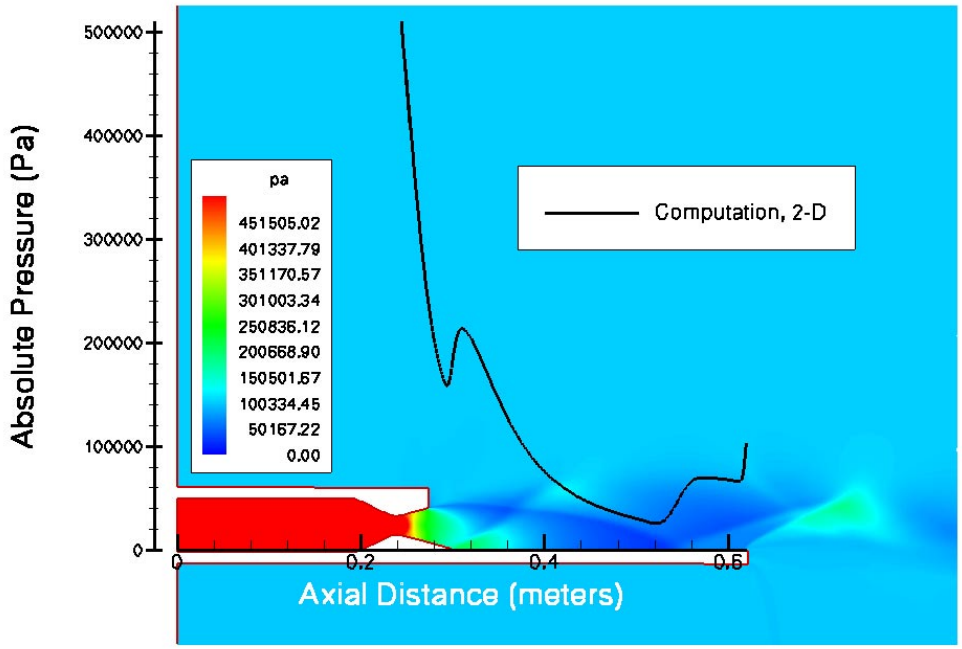

(c) Pc250 – Combustion Chamber Pressure = 250 psia

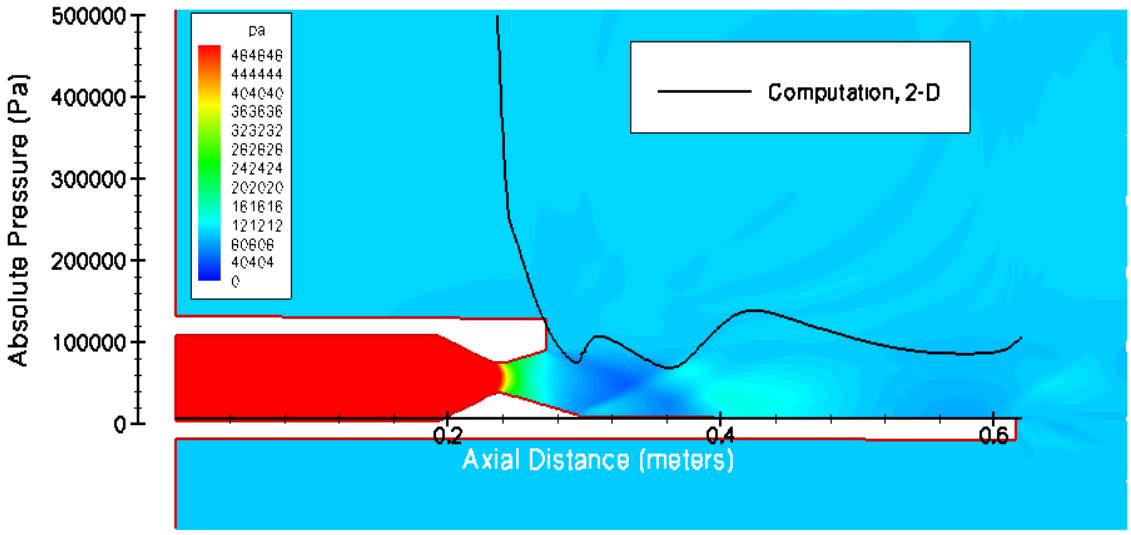

(d) Pc130 – Combustion Chamber Pressure = 130 psia

Figure 22 (c-d). Pressure contours and pressure distribution along the wall for Pc130 and Pc250 cases

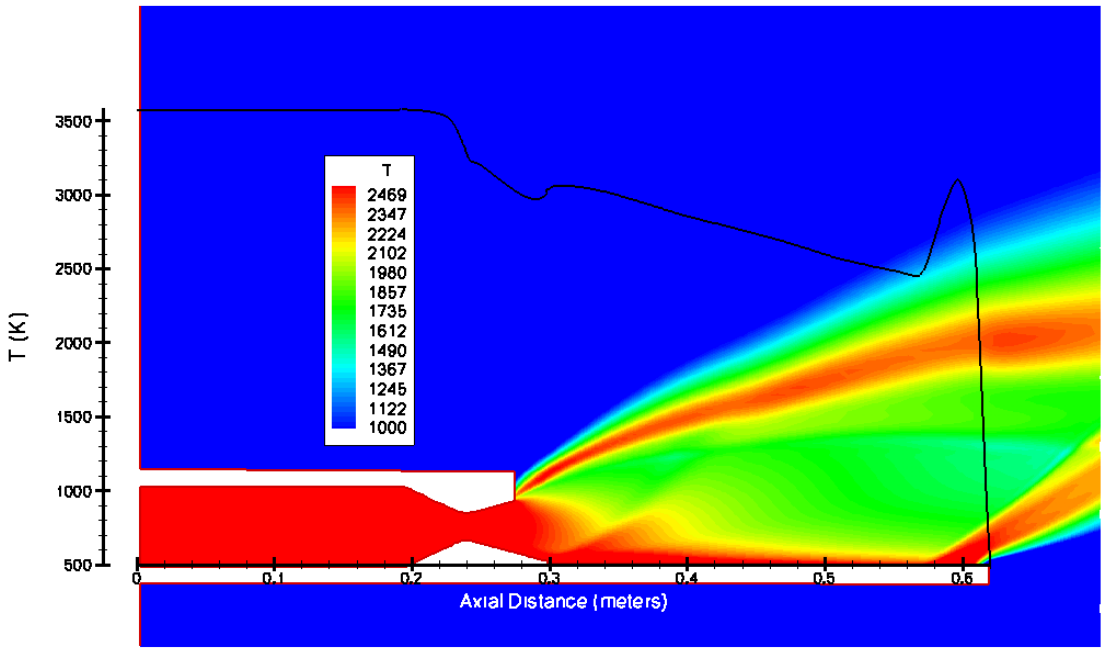

(a) Pc500 – Combustion Chamber Pressure = 500 psia

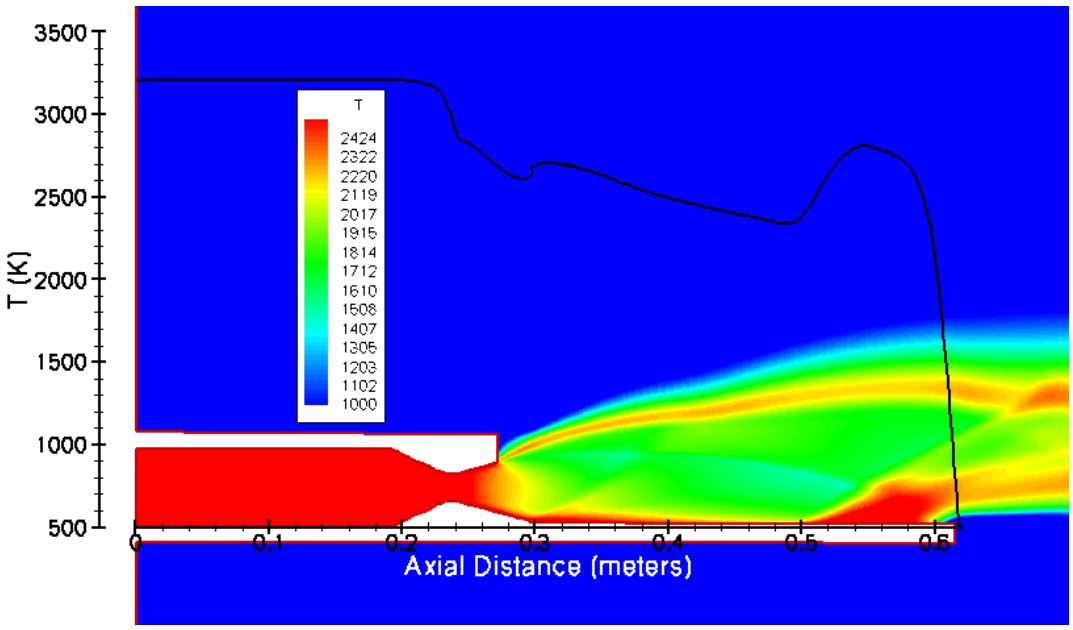

(b) Pc300 – Combustion Chamber Pressure = 300 psia

Figure 23 (a-b). Temperature contours and temperature distribution along the wall for Pc300 and Pc500 cases

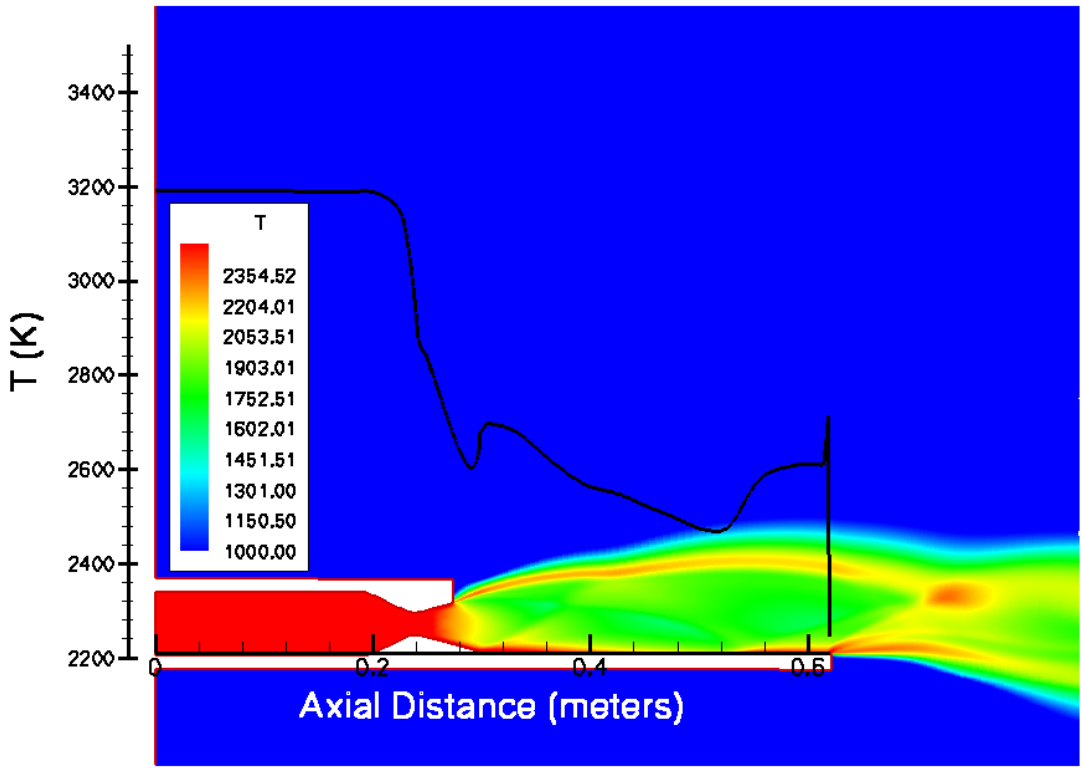

(c) Pc250 – Combustion Chamber Pressure = 250 psia

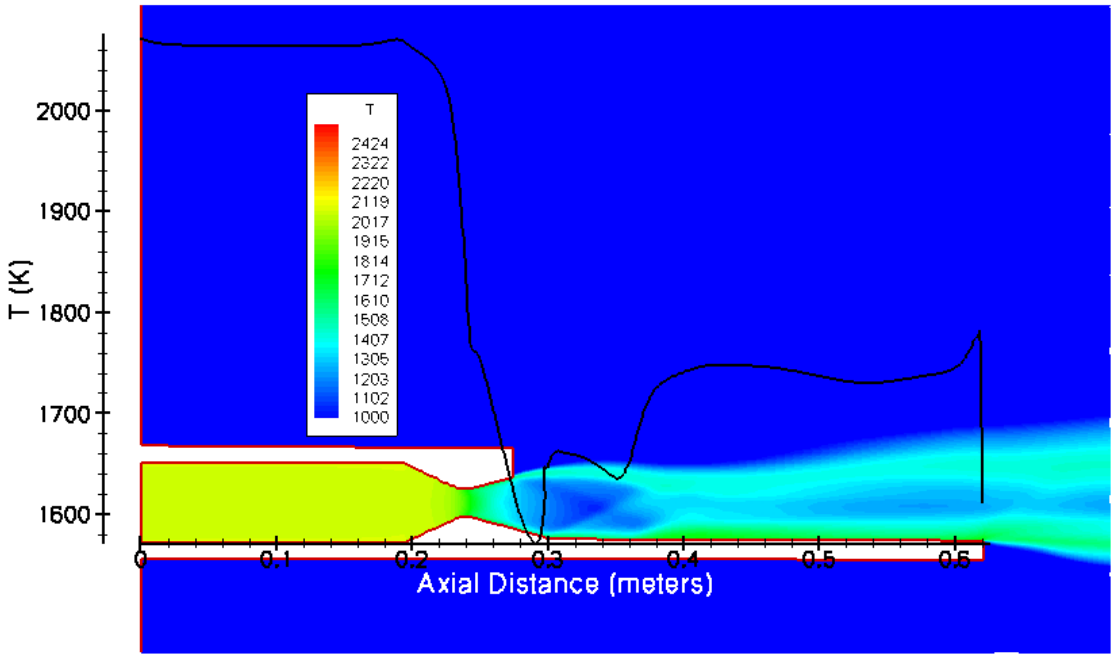

(d) Pc130 – Combustion Chamber Pressure = 130 psia

Figure 23 (c-d). Temperature contours and temperature distribution along the wall for Pc130 and Pc250 cases

8. The Related Experimental Measurements

For the 3-D, water-cooled test rig (see Figure 1), pressure and temperature values are measured at several locations for the four chamber conditions presented above [3]. Pressure is measured at three locations along the two sidewalls immediately above the flat panel. The vertical sidewalls, looking upstream, are termed here the right wall and the left wall. Temperature on the surface of the flat panel (calorimeter) is measured via thermocouples located on three rows, along the surface, with each row containing three points.

A 2-D drawing [3] showing the approximate locations at which pressure and temperature measurements are made is shown in Figure 24.

Computational and the related experimental results are tabulated in Tables 3 through 10. Comparison of the computed pressure distribution on the surface of the flat panel and the related measurement is shown in Figures 21 (a) to (c). The computed temperature distribution on the flat panel and its related measurement is given in Figures 25 (a) to (c). As mentioned above, the measured temperature values on the panel are those of the solid copper (except for Case Pc250 where a less conductive composite material is used) which is cooled via the flow of high pressure water (900 psia) through channels drilled inside the copper flat panel [2], whereas the computed values are for the hot gas flow above the panel and assuming the adiabatic wall condition. Nevertheless, the computed results clearly demonstrate the trend.

It should be recognized that the numerical simulation is 2-D and the possible 3-D effects that may be important are not considered in the computations.

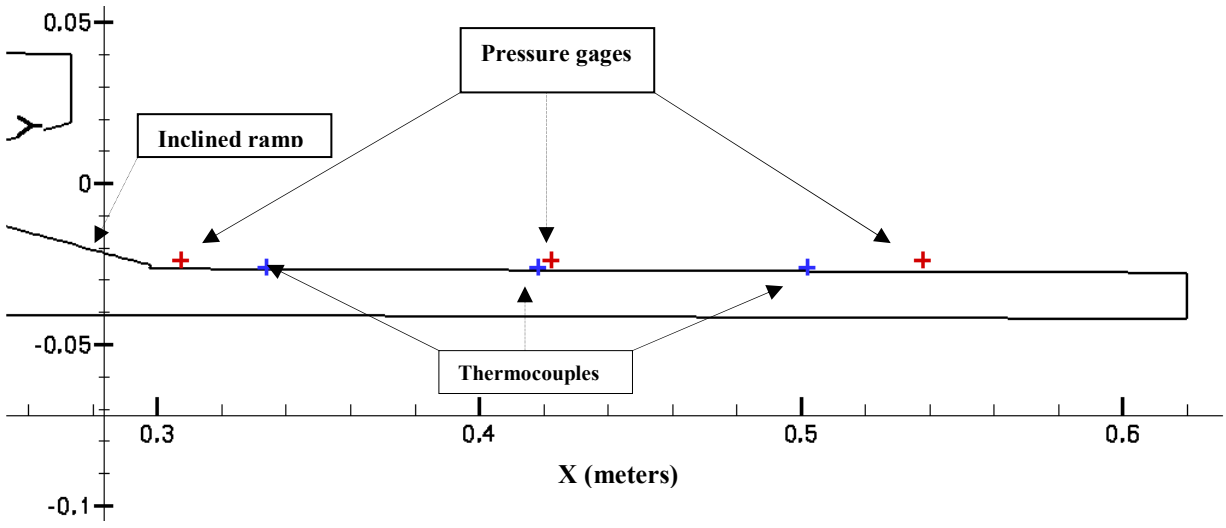

Figure 24. Position of the thermocouples and the pressure gages on the surface of the flat panel (calorimeter) and on the sidewalls

Table 3. Experimental and computational pressure for the Case Pc130
Measurement: 3-D and cooled walls
Computation: 2-D and adiabatic

PRESSURE PORTS	X *(meters)*	Y*(meters)*	Z*(meters)*	*ABS. PRESSURE MEASURED (Pa)*	*ABS. PRESSURE COMPUTED (Pa)*
IP1 *(left wall)*	0.3073	-0.0234	-0.02921	89882.68	100179.34
IP4 *(right wall)*	0.3073	-0.0234	0.02921	92478.21	
IP2 *(left wall)*	0.4229	-0.0234	-0.02921	161943.04	131969.20
IP5 *(right wall)*	0.4229	-0.0234	0.02921	153265.97	
IP3 *(left wall)*	0.5384	-0.0234	-0.02921	85611.01	88286.70
IP6 *(right wall)*	0.5384		0.02921	83578.43	

Table 4. Experimental and computational temperature for the Case Pc130
Measurement: 3-D and cooled walls
Computation: 2-D and adiabatic

THERMOCOUPLES	X*(meters)*	Y*(meters)*	Z*(meters)*	*AVG. TEMPERATURE MEASURED (°K) (top surface of the flat panel)*	*TEMPERATURE COMPUTED (°K) (top surface hot gas adiabatic wall)*
TC13	0.334	-0.0267	-0.01905	360.60	1650.15
TC14	0.334	-0.0267	0.0		
TC15	0.334	-0.0267	0.01905		
TC16	0.41839	-0.0267	-0.01905	406.1	1742.49
TC17	0.41839	-0.0267	0.0		
TC18	0.41839	-0.0267	0.01905		
TC19	0.50218	-0.0267	-0.01905	395.9	1695.16
TC20	0.50218	-0.0267	0.0		
TC21	0.50218	-0.0267	0.01905		

Table 5. Experimental and computational pressure for the Case Pc250
Measurement: 3-D and cooled walls
Computation: 2-D and adiabatic

PRESSURE PORTS	X *(meters)*	Y*(meters)*	Z*(meters)*	*ABS. PRESSURE MEASURED (Pa)*	*ABS. PRESSURE COMPUTED (Pa)*
IP1	0.3073	-0.0234	-0.02921	107558.00	203054
IP4	0.3073	-0.0234	0.02921	103422.00	
IP2	0.4229	-0.0234	-0.02921	78600.00	58062
IP5	0.4229	-0.0234	0.02921	73084.59	
IP3	0.5384	-0.0234	-0.02921	88942.57	37081
IP6	0.5384	-0.0234	0.02921	90321.52	

Table 6. Experimental and computational temperature for the Case Pc300
Measurement: 3-D and cooled walls
Computation: 2-D and adiabatic

THERMOCOUPLES	X*(meters)*	Y*(meters)*	Z*(meters)*	*AVG. TEMPERATURE MEASURED (°K) (top surface of the flat panel)*	*TEMPERATURE COMPUTED (°K) (top surface hot gas adiabatic wall)*
TC13	0.334	-0.0267	-0.01905	1718.33	
TC14	0.334	-0.0267	0.0		2664.42
TC15	0.334	-0.0267	0.0254		
TC16	0.41839	-0.0267	-0.01905	1420.00	
TC17	0.41839	-0.0267	0.0		2389.63
TC18	0.41839	-0.0267	0.0254		
TC19	0.50218	-0.0267	-0.01905	1222.78	
TC20	0.50218	-0.0267	0.0		2220.93
TC21	0.50218	-0.0267	0.0254		

Table 7. Experimental and computational pressure for the Case Pc300
Measurement: 3-D and cooled walls
Computation: 2-D and adiabatic

PRESSURE PORTS	X *(meters)*	Y*(meters)*	Z*(meters)*	*ABS. PRESSURE MEASURED (Pa)*	*ABS. PRESSURE COMPUTED (Pa)*
IP1	0.3073	-0.0234	-0.02921	223579.55	239789.00
IP4	0.3073	-0.0234	0.02921	176508.25	
IP2	0.4229	-0.0234	-0.02921	77957.82	69217.40
IP5	0.4229	-0.0234	0.02921	83290.92	
IP3	0.5384	-0.0234	-0.02921	56738.26	66336.50
IP6	0.5384	-0.0234	0.02921	79069.25	

Table 8. Experimental and computational temperature for the Case Pc300
Measurement: 3-D and cooled walls
Computation: 2-D and adiabatic

THERMOCOUPLES	X*(meters)*	Y*(meters)*	Z*(meters)*	*AVG. TEMPERATURE MEASURED (°K) (top surface of the flat panel)*	*TEMPERATURE COMPUTED (°K) (top surface hot gas adiabatic wall)*
TC13	0.334	-0.0267	-0.01905	483.22	
TC14	0.334	-0.0267	0.0		2683.69
TC15	0.334	-0.0267	0.0254		
TC16	0.41839	-0.0267	-0.01905	361.85	
TC17	0.41839	-0.0267	0.0		2457.97
TC18	0.41839	-0.0267	0.0254		
TC19	0.50218	-0.0267	-0.01905	344.83	
TC20	0.50218	-0.0267	0.0		2354.68
TC21	0.50218	-0.0267	0.0254		

Table 9. Experimental and computational pressure for the Case Pc500
Measurement: 3-D and cooled walls
Computation: 2-D and adiabatic

PRESSURE PORTS	X *(meters)*	Y*(meters)*	Z*(meters)*	*ABS. PRESSURE MEASURED (Pa)*	*ABS. PRESSURE COMPUTED (Pa)*
IP1	0.3073	-0.0234	-0.02921	288744.12	399950.00
IP4	0.3073	-0.0234	0.02921	399196.99	
IP2	0.4229	-0.0234	-0.02921	149621.39	116566.20
IP5	0.4229	-0.0234	0.02921	127154.09	
IP3	0.5384	-0.0234	-0.02921	79851.12	46630.60
IP6	0.5384	-0.0234	0.02921	68947.73	

Table 10. Experimental and computational temperature for the Case Pc500
Measurement: 3-D and cooled walls
Computation: 2-D and adiabatic

THERMOCOUPLES	X*(meters)*	Y*(meters)*	Z*(meters)*	*AVG. TEMPERATURE MEASURED (°K) (top surface of the flat panel)*	*TEMPERATURE COMPUTED (°K) (top surface hot gas adiabatic wall)*
TC13	0.334	-0.0267	-0.01905	483.22	
TC14	0.334	-0.0267	0.0		2683.69
TC15	0.334	-0.0267	0.01905		
TC16	0.41839	-0.0267	-0.01905	361.85	
TC17	0.41839	-0.0267	0.0		2457.97
TC18	0.41839	-0.0267	0.01905		
TC19	0.50218	-0.0267	-0.01905	344.83	
TC20	0.50218	-0.0267	0.0		344.83
TC21	0.50218	-0.0267	0.01905		

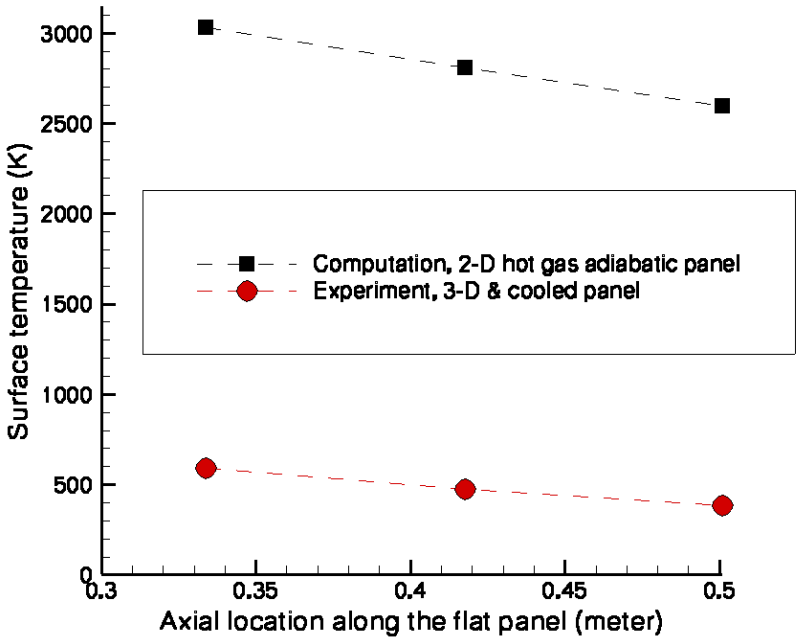

(a) Pc500 Case

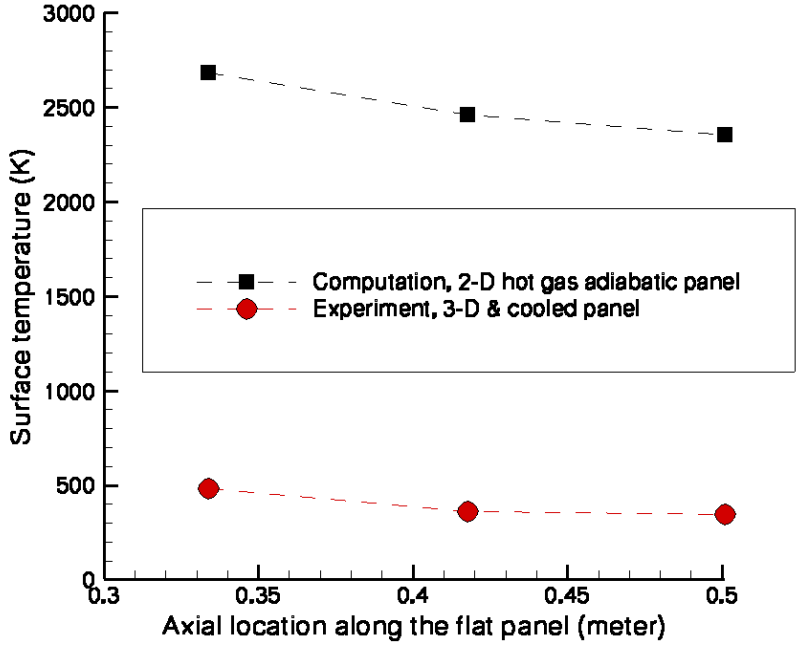

(b) Pc300 Case

Figure 25 (a-b). Experimental and computational temperature along the flat panel for Pc300 and Pc500 cases

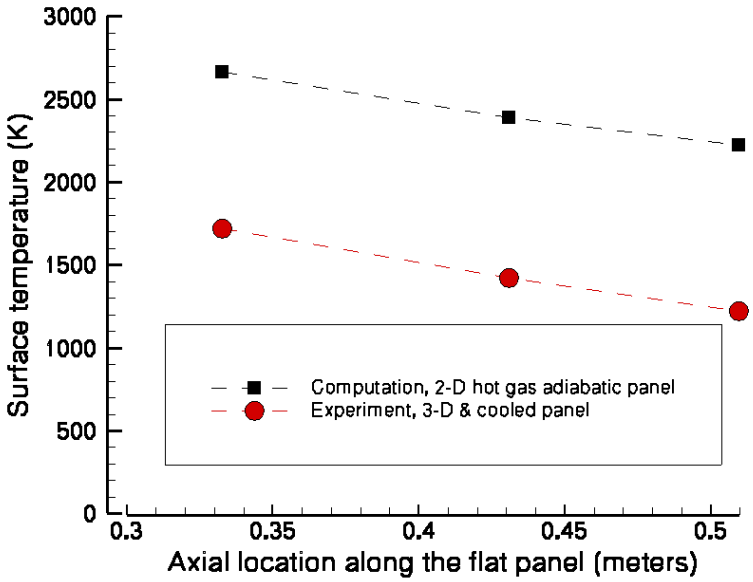

(c) Pc250 Case

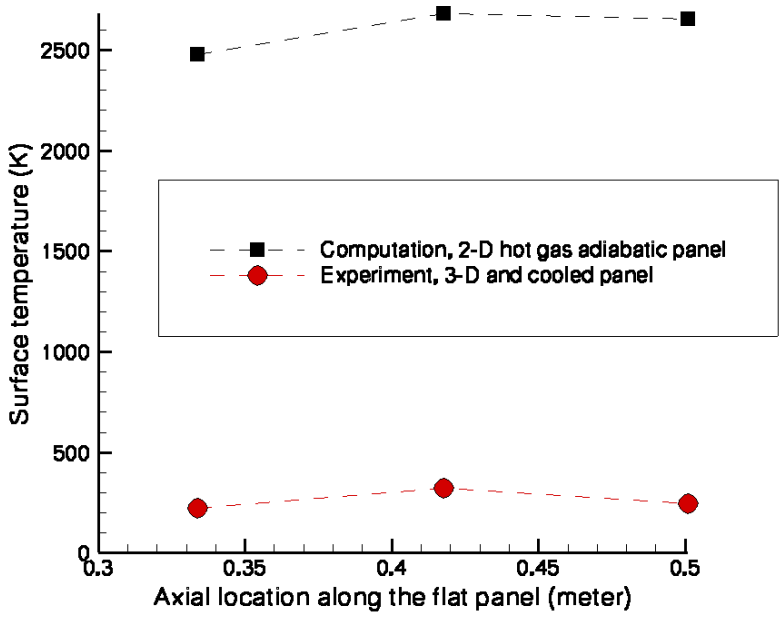

(d) Pc130 Case

Figure 25 (c-d). Experimental and computational temperature along the flat panel for Pc130 and Pc250 cases

9. Conclusions and Suggested Future Plans

Two-dimensional Euler and Navier-Stokes simulations are performed to obtain the flow field induced through a rocket thruster of Cell 22 at NASA Glenn Research Center, using the NCC code.

The simulations have captured details of the flow field, such as the plume formation and expansion, formation of the shock waves and their effects on the temperature and pressure distributions on the walls. The effect of the viscous boundary layer on the wall temperature is clearly demonstrated, and consequences of using more simplified models such as the method of characteristics (MOC) or the inviscid-flow assumption are evident.

The present study determines the appropriate parameters (i.e. boundary conditions, proximity of the boundaries to the thruster and the panel attached to it, the grid resolution, etc.) for the set-up and successful execution of the NCC code. The two-dimensional domain was chosen, for fast turn-around, minimizing computational requirements and for determination of these parameters. Once these parameters are determined, change in any of them can be accommodated with relative ease in the future runs.

Despite the fact that the computations were performed on a 2-D grid and the walls are adiabatic, the comparison of the computed and the related measurements for 3-D and cooled walls showed that the results of the simulations are consistent with those obtained from the related rig tests. To compute effects of the wall cooling on the temperature distribution and to calculate the heat fluxes on the cooled flat panel requires implementation of a conjugate heat transfer into the code. Efforts are being undertaken to incorporate this option.

Using the knowledge gained from the 2-D results, it is suggested to expand the simulations to a 3-D domain. The 3-D computations will consider the effects of the sidewalls on the flow field, shock waves, and the pressure/temperature distributions on the walls. Furthermore, a conjugate heat transfer calculation will provide heat fluxes between the gaseous fluid and the solid boundaries of the flat panel and will give temperature distribution on the flat panel.

References

1. Liu, N.-S., “On the Comprehensive Modeling and Simulation of Combustion Systems,” AIAA 2001–0805, 39th AIAA Aerospace Sciences Meeting and Exhibit, January 8–11, 2001, Reno, NV.
2. Stout, J.B., “Testing of Check Sample and Three Section Calorimeter in Cell 22 at NASA Glenn Research Center, Summary of Aeroconvective and Thermal Analysis,” Boeing – Rocketdyne Propulsion and Power System 1999.
3. Linne, L.D. and Dickens, K., Private communications, June 2002.

REPORT DOCUMENTATION PAGE

Form Approved
OMB No. 0704-0188

1. AGENCY USE ONLY (*Leave blank*)	2. REPORT DATE	3. REPORT TYPE AND DATES COVERED
	May 2003	Technical Memorandum

4. TITLE AND SUBTITLE

Simulation of the Flow Field Associated With a Rocket Thruster Having an Attached Panel

5. FUNDING NUMBERS

WBS–22–713–10–06

6. AUTHOR(S)

Farhad Davoudzadeh and Nan-Suey Liu

7. PERFORMING ORGANIZATION NAME(S) AND ADDRESS(ES)

National Aeronautics and Space Administration
John H. Glenn Research Center at Lewis Field
Cleveland, Ohio 44135–3191

8. PERFORMING ORGANIZATION REPORT NUMBER

E–13935

9. SPONSORING/MONITORING AGENCY NAME(S) AND ADDRESS(ES)

National Aeronautics and Space Administration
Washington, DC 20546–0001

10. SPONSORING/MONITORING AGENCY REPORT NUMBER

NASA TM—2003-212347

11. SUPPLEMENTARY NOTES

Prepared for the 2003 Fluids Engineering Division Summer Meeting cosponsored by the American Society of Mechanical Engineers and the Japan Society of Mechanical Engineers, Honolulu, Hawaii, July 6–10, 2003. Farhad Davoudzadeh, University of Toledo, Toledo, Ohio 43606; Nan-Suey Liu, NASA Glenn Research Center. Responsible person, Nan-Suey Liu, organization code 5830, 216–433–8722.

12a. DISTRIBUTION/AVAILABILITY STATEMENT

Unclassified - Unlimited
Subject Categories: 07 and 20 Distribution: Nonstandard

Available electronically at http://gltrs.grc.nasa.gov

This publication is available from the NASA Center for AeroSpace Information, 301–621–0390.

12b. DISTRIBUTION CODE

13. ABSTRACT ***(Maximum 200 words)***

Two-dimensional inviscid and viscous numerical simulations are performed to predict the flow field induced by a H_2-O_2 rocket thruster and to provide insight into the heat load on the articles placed in the hot gas exhaust of the thruster under a variety of operating conditions, using the National Combustion Code (NCC). The simulations have captured physical details of the flow field, such as the plume formation and expansion, formation of the shock waves and their effects on the temperature and pressure distributions on the walls of the apparatus and the flat panel. Comparison between the computed results for 2-D and adiabatic walls and the related experimental measurements for 3-D and cooled walls shows that the results of the simulations are consistent with those obtained from the related rig tests.

14. SUBJECT TERMS

H_2-O_2 rocket thruster; Plume; Heat load

15. NUMBER OF PAGES

37

16. PRICE CODE

17. SECURITY CLASSIFICATION OF REPORT	18. SECURITY CLASSIFICATION OF THIS PAGE	19. SECURITY CLASSIFICATION OF ABSTRACT	20. LIMITATION OF ABSTRACT
Unclassified	Unclassified	Unclassified	